Ancient Hybridization Patterns Between Bighorn and Thinhorn Sheep

Sarah H. D. Santos, Rhiannon M. Peery, Joshua M. Miller, Anh Dao, Feng-Hua Lyu, Xin Li, Meng-Hua Li, David W. Coltman

Ancient hybridization patterns between bighorn and thinhorn sheep

Running title

Introgression among Pachyceriform genomes

Sarah H. D. Santos[1], Rhiannon M. Peery[1], Joshua M. Miller[1], Anh Dao[1], Feng-Hua Lyu[2], Xin Li[3,4], Meng-Hua Li[3], David W. Coltman[1]

[1] Department of Biological Sciences, University of Alberta, Edmonton, AB, Canada

[2] College of Animal Science and Technology, China Agricultural University, Beijing 100193, China

[3] CAS Key Laboratory of Animal Ecology and Conservation Biology, Chinese Academy of Sciences (CAS), Beijing 100101, China

[4] University of Chinese Academy of Sciences (UCAS), Beijing, China

Corresponding author: Sarah Santos (sarahhel@ualberta.ca)

Abstract

Whole-genome sequencing has advanced the study of species evolution, including the detection of genealogical discordant events such as ancient hybridization and incomplete lineage sorting (ILS). The evolutionary history of bighorn (*Ovis canadensis*) and thinhorn (*Ovis dalli*) sheep present an ideal system to investigate evolutionary discordance due to their recent and rapid radiation and putative secondary contact between bighorn and thinhorn sheep subspecies, specifically the dark pelage Stone sheep (*O. dalli stonei*) and predominately white Dall sheep (*O. dalli dalli*), during the last ice age. Here we used multiple genomes of bighorn and thinhorn

sheep, together with snow (*O. nivicola*) and the domestic sheep (*O. aries*) as outgroups, to assess their phylogenomic history, potential introgression patterns and their adaptive consequences. Among the Pachyceriforms (snow, bighorn and thinhorn sheep) a consistent monophyletic species tree was retrieved; however, many genealogical discordance patterns were observed. Alternative phylogenies frequently placed Stone and bighorn as sister clades. This relationship occurred more often and was less divergent than that between Dall and bighorn. We also observed many blocks containing introgression signal between Stone and bighorn genomes in which coat color genes were frequently present. Introgression signals observed between Dall and bighorn were more random and less frequent, and therefore probably due to ILS or intermediary secondary contact. These results strongly suggest that Stone sheep originated from a complex series of events, characterized by multiple, ancient periods of secondary contact with bighorn sheep.

Keywords

Gene Flow; Natural Selection; Coat Color Genes; Melanogenesis; Adaptive Introgression; *Ovis* spp.

Introduction

Vertical transmission of genomic information does not always offer a complete picture of the evolutionary history of species. Gene trees are often discordant from species trees, and mechanisms leading to discordance, such as hybridization and incomplete lineage sorting (ILS), are missed due to a lack of comprehensive genomic sequences (Bravo et al., 2019; Payseur & Rieseberg, 2016). The advancement of high-throughput whole-genome sequencing technologies

and computation efficiency has brought new opportunities for understanding how speciation has happened throughout time (Bravo et al., 2019; Ekblom & Wolf, 2014; Kulski, 2016). The ever-increasing amount of whole-genome data, specifically for non-model species, has revealed remarkable patterns of gene flow blocks, evidence for introgression, in both extant and extinct species (e.g., Barlow et al., 2018; Edelman et al., 2019; Fontaine et al. 2015; Kumar et al. 2017; Li, Figueiro, Eizirik, & Murphy, 2019a; Palkopoulou et al., 2018; Vianna et al., 2020). Within these lineages, numerous conflicting signals can be observed among genomic regions, including historical encounters of distinct species and their posterior hybridization and genomic incorporation (Degnan & Rosenberg, 2009; Payseur & Rieseberg, 2016; Shurtliff, 2013).

Gene flow blocks arising through introgression are more often detected in species with recent and rapid radiations, in which insufficient time has passed to erase the introgression signal (Degnan & Rosenberg, 2009; Payseur & Rieseberg, 2016). *Ovis* spp. present an opportunity to explore a recent divergence of approximately 8.31 million years ago (Ma) (Lv et al., 2015), and the effects of genomic introgression among these taxa. Their diversification has resulted in eight species divided into two major clades, the Pachyceriforms and Argaliforms/Moufloniforms (Bunch, Wu, Zhang, & Wang, 2006; Dotsev et al., 2019; Geist, 1971; Rezaei et al., 2010). *Ovis* phylogenies have been extensively studied using a variety of molecular markers, in which some remarkable genomic footprints left by admixture events were observed. However, the majority of these studies have focused on understanding the origin of domesticated sheep breeds (*O. aries*; Bunch et al., 2006; Hiendleder, Kaupe, Wassmuth, & Janke, 2002; Hu et al., 2018), and on hybridization between wild and domesticated sheep species (Deng et al., 2020; Feulner et al., 2013; Gratten et al., 2010; Lv et al., 2015; Rochus et al., 2018; Rochus, Westberg Sunesson, Jonas, Mikko, & Johansson, 2019; Somenzi, Ajmone-Marsan, & Barbato, 2020). Such

hybridization events can be followed by an adaptive introgression process (Hedrick, 2013), especially concerning coat color in sheep (Hu et al., 2018; Rochus et al., 2018, 2019).

Within the *Ovis* species complex, the Pachyceriforms compromise a monophyletic clade of three species (Bunch et al., 2006; Rezaei et al., 2010): thinhorn sheep (*O. dalli*), with its two subspecies Dall (*O. dalli dalli*) and Stone (*O. dalli stonei*), form an inner clade with bighorn (*O. canadensis*) followed by snow sheep (*O. nivicola*) as their sister-group (Bunch et al., 2006; Geist, 1971; Rezaei et al., 2010) (Figure 1). Though this species-level topology is generally agreed upon, the relationship between thinhorn and bighorn is likely tangled with potential gene flow events (Loehr, Carey, Ylonen, & Suhonen, 2008; Loehr et al., 2006), making the Pachyceriforms a compelling group in which to study ancient admixture and its adaptive consequences. Notably, it is hypothesized that admixture events contributed to the dark coat color pattern seen in Stone sheep (Figure 1a-b), while Dall's ancestor (Loehr et al., 2006, 2008), which was isolated in the Alaskan refugium, developed its white coat color (Figure 1c) (Klein, 1965). While bighorn and thinhorn may have experienced gene flow in the past, they have distinct contemporary distributions: bighorn sheep are widely distributed in western North America as far north as the Rocky Mountains in British Columbia and Alberta (Festa-Bianchet, 2020a). Thinhorn sheep are found in more northerly regions of North America, and their subspecies ranges overlap. Dall sheep are found in Alaska, the Northwest Territories, the Yukon and in northwest British Columbia. Stone's sheep are endemic to northern British Columbia, overlapping with Dall sheep along the Yukon border where they are admixed. (Festa-Bianchet, 2020b; Sim et al., 2016).

To date, no work has used whole-genome sequences to reveal the ancient admixture processes that might have happened between bighorn and thinhorn sheep. By comparing genomic sequences from multiple individuals of each species, we were able to trace their evolutionary

history back to when ancient admixture took place and infer how introgression has impacted their speciation and shaped their genome composition.

Materials and Methods

Whole-genome assessment

Data acquisition and filtering

Whole-genome sequencing data of bighorn and thinhorn sheep (Table S1) were obtained from an unpublished work (Chen, Xu, & Li, unpublished). These samples were collected in native areas in the USA and Canada (Table S1). Five bighorn individuals were from Montana and one from Alberta. The two subspecies of thinhorn comprised three Stone individuals from British Columbia, and one Dall from the Northwest Territories. After obtaining genomic DNA from blood using standard phenol-chloroform extraction procedure, TruSeq PCR-free preparation kits (Illumina, San Diego, CA) were used to construct paired-end sequencing libraries with an insert size of approximately 350-bp. Whole-genomes were sequenced on the Illumina HiSeq X Ten Sequencer (Illumina Inc.).

We used the bighorn (N=6) and thinhorn (N=4) genomic data, together with publicly available short-read sequences of snow sheep (Upadhyay et al., 2020) and goat (*Capra hircus*) (Table S1). All reads were checked for quality using FastQC v.0.11.8 (Andrews, 2019). For the bighorn and thinhorn data, quality filters were applied to all paired-end reads obtained by excluding reads with unidentified nucleotides (N-content) ≥10, more than 10 nucleotides aligned to the adaptor or mismatches >10%, more than 50% of read bases with Phred quality score (Q-score) less than 5, and putative PCR duplicates generated in the library construction process (Chen, Xu & Li, unpublished). No adaptors were kept. We verified that the snow sheep had

short-reads within the 20-30 phred-score range. For the goat short-read data, which we used as outgroup, we trimmed lower quality reads (phred-score <20) and sequences with length smaller than 50-bp with Trimmomatic v.39 (Bolger, Lohse, & Usadel, 2014). We used BBMap v.38.87 (Bushnell, 2020) to check and fix paired-end reads' order. All individuals were mapped against the domestic sheep genome, which includes 26 autosomes plus the X chromosome (NCBI accession no. GCA_002742125.1; Oar_rambouillet_v1.0), using BWA-MEM v.0.7.17 with default parameters (Li & Durbin, 2009). The mapped short-read data of each individual was further filtered, sorted, indexed, and their mapping success was checked with Samtools v.1.10 (Li et al., 2009). The overall depth (Table S1) and per base coverage for each individual (Figure S1) were retrieved by employing Samtools and BEDTools v.2.29.2 (Quinlan & Hall, 2010), respectively. Finally, we obtained a pseudohaploid consensus for each genome using ANGSD v.0.929 (*doFasta* 2; Korneliussen, Albrechtsen, & Nielsen, 2014), in which we applied quality filters (*minMapQ* 30; *minQ* 20; *setMinDepth* 5). Each nucleotide was determined randomly, coming from either strands, by considering the number of base counts. These consensus sequences, from bighorn, snow, thinhorn and goat, were masked for repetitive regions based on the domestic sheep coordinates with BEDTools.

Dataset generation

Nuclear whole-genomes were separated into genomic fragments (GF) to perform the following analyses. Alignments of 16 different datasets (128 subsets) were built using a custom python script (Figueiro, 2019), depending on the individuals used and analyses done (Table 1; Figure S2-S8). We generated non-overlapping 10-kb GFs (no step size) with BEDTools for each focal species (bighorn and thinhorn sheep) to estimate their nucleotide diversity (Dataset 1: Table

1). Furthermore, we generated GFs of 1-Mb (Dataset 2), 100-kb (Dataset 3), and 10-kb (Dataset 4) for the phylogenomic analyses (Table 1). We set step sizes between GF either 6-kb or 100-kb to compensate for possible biases due to the extent of linkage disequilibrium (Kijas et al., 2014) or recombination (Xin et al., 2020), respectively. We also included a bigger step size (200-kb) and to test whether the same signal was obtained. To investigate the full spectrum of the evolutionary history, Datasets 2-4 included six bighorn, four thinhorn, and one snow sheep, plus the domestic sheep as the outgroup. We then focused on datasets that allowed for fine scale comparisons of 10-kb GFs, using the step sizes described previously (Datasets 5-7: Table 1). Datasets 5 and 6 had the same ingroup individuals (N=6) except for the addition of the goat as the outgroup in Dataset 6 (N=7). Dataset 7 had only one individual of each species/subspecies (Table 1; N=5) and used the domestic sheep as an outgroup. We used trimAl v.1.4.rev22 (Capella-Gutierrez, Silla-Martinez, & Gabaldon, 2009) in Datasets 1-7 to filter spurious sequences that included missing data in more than 20% of sequences (*gt* 0.8), and only considered alignments with 50% or more sequence retained. For the introgression analyses, we generated and used all non-overlapping windows of 100-kb with no step size (Datasets 8-16: Table 1; Figure S2-S8). We organized subsets within each dataset for the 5- (Datasets 8-13: Figure S2-S7) and 4-taxon (Datasets 14-16: Figure S8) introgression analyses, differing in the bighorn and thinhorn individuals included.

Population assessment

To assess the population structure of bighorn (N=6) and thinhorn (Dall N=1; Stone N=3) individuals, a haplotype-based variant call of the whole mapped genomes was done with default parameters in Platypus v.0.8.1 (Rimmer et al., 2014). We performed a PCA with Plink v.2.0

(Chang et al., 2015; Purcell & Chang, 2019) and applied quality filters that included a threshold of 0.1 for missing call frequency of variants and samples. These results were compared to their collection site (Table S1). Results were visualized with the R package ggplot2 v.3.3.2 (Wickham, 2016).

Additionally, we estimated the diversity of each focal species by calculating diversity per nucleotide site (π) per focal species using the python egglib v.3.0.0 package (De Mita & Siol, 2012). Here we employed Dataset 1 alignments (all bighorn and thinhorn individuals separately; Table 1) with non-overlapping 10-kb GFs, and differences per window were divided by the effective number of analyzed sites within each GF. Only windows present in all sequences were considered. Lastly, we performed an outlier test, which removed windows with excessive π values falling more than 1.5 times the interquartile range above the third quartile or below the first quartile.

The filtered values obtained for thinhorn and bighorn were compared statistically using IBM SPSS Statistics v.27 (IBM Corp., 2020). The windows were separated into all chromosomes, autosomes, and the X chromosome, all of which were tested for normality with a Kolmogorov-Smirnov test. We also visualized whether the distribution was normal by verifying the histogram and Q-Q plot. We applied the non-parametric Mann-Whitney U test to compare diversity values of each data partition and compared autosomes to the X-chromosome of each species separately. In all scenarios, we used a p-value threshold of 0.05.

Phylogenomic analyses

Gene tree estimation and species tree reconstruction

We employed a maximum-likelihood method (RAxML-MPI v.8.2.12) (Stamatakis, 2014) to infer phylogenomic trees for each GF in their respective Datasets (2-7) (Table 1). We used the rapid bootstrap estimation using 100 replicates. We applied the GTRGAMMA substitution model, since RAxML was designed to handle parameter rich models of GTR (Stamatakis, 2014). All other parameters were kept at default. The results of Datasets 5-7 (each with fewer and more representative individuals) were summarized using Newick Utilities v.1.6 (Junier & Zdobnov, 2010), considering specific evolutionary relationships among thinhorn and bighorn (Figure 1d-f). These topologies were constrained to vary the sister relationships of bighorn and thinhorn individuals, whereas the domestic and snow sheep (as well as goat in Dataset 6) remained as outgroups (topologies outside of this were called "Other Topologies"). We focused on topologies that represented the original speciation event (topology 1), as well as topologies that placed Stone (topologies 2 and 3) or Dall (topologies 4 and 5) as sister to bighorn (Figure 1d-f). The nodal supports of our main topologies were verified based on a >70 threshold, where we counted the number of windows representing a specific phylogenetic relationship (e.g., Stone and bighorn as sisters). Additionally, we tested whether using the goat genome as an outgroup would impact the phylogenomic inferences of Dataset 6 and compared these results to Dataset 5.

The resulting trees (topologies 1-5 and other topologies) from Datasets 5-7 were used to generate consensus species trees for all chromosomes, autosomes, and the X chromosome using Astral-III (Zhang, Rabiee, Sayyari, & Mirarab, 2018). First, we obtained unrooted trees with ape v.5.4-1 in R (Paradis & Schliep, 2019), followed by estimating the species trees for each dataset and partition. All parameters in Astral were kept at default.

Divergence time estimation

To characterize patterns of divergence across the genomes, we estimated their species tree divergence times with BPP v.4.3.0 (Flouri, Jiao, Rannala, & Yang, 2018), a multispecies coalescent (MSC) model method that considers the presence of incomplete lineage sorting (ILS). Here we employed Dataset 5 alignments (Step sizes: 100 and 200-kb) that resulted in the species tree rooted by the domestic sheep. This dataset was chosen to fulfill the requirements of BPP, which included at least two individuals of our focal group (thinhorn and bighorn sheep). We applied the A00 model that estimates the parameters based on a given species tree model. The mitogenome estimation of the sheep root age (8.31 Ma; Lv et al., 2015) was used as the inverse-gamma prior (3, 0.01662). The *burnin*, *samplefreq*, and *nsample* parameters were set to 10000, 20, and 20000, respectively. All other parameters were left default, and convergence was verified with Tracer v.1.7.1 (Rambaut, Drummond, Xie, Baele, & Suchard, 2018). The results were then recalibrated based on the 8.31 Ma root age.

We investigated speciation among our focal species by estimating the absolute divergence per site (d_{xy}) between thinhorn and bighorn using a python egglib package. Here we explored the relationship and potential hybridization events between Stone and bighorn, considering how divergent Dall or Stone were from bighorn. We used Dataset 5, in which bighorn individuals were from different locations (Table S1), to consider the impact of having distinct intraspecific demographic histories. One individual (B4) was from the National Bison Range, a population that experienced intraspecific admixture after intentional introduction of individuals to perform a 'genetic rescue' (Hogg, Forbes, Steele, & Luikart, 2006; Miller et al., 2014; Miller, Poissant, Hogg, & Coltman, 2012). The other individual (B6) originated from Ram Mountain, which is an isolated, native population with no historical intraspecific admixture (Coltman, Festa-Bianchet, Jorgenson, & Strobeck, 2002; Miller et al., 2014). We divided the differences obtained for each

231 combination of species (Dall or Stone *vs*. bighorn) by the effective number of analyzed sites
232 within each GF. To compare their d_{xy}, we only considered windows present in all comparisons.
233 Additionally, we performed an outlier test, and these results were tested for normality and
234 significance, in the same manner as described for nucleotide diversity. We compared the results
235 for all chromosomes, autosomes, and the X chromosome, considering an alpha value of 0.05.
236
237 Ancient hybridization pattern estimation
238 *Reticulate evolution evaluation*
239 Considering the likely reticulate evolutionary events in the speciation of these taxa, we
240 further estimated the phylogenomic signal in the presence of hybridization and ILS by employing
241 PhyloNet (Than, Ruths, & Nakhleh, 2008; Wen, Yu, Zhu, & Nakhleh, 2018). The species
242 networks were inferred from gene trees that included bootstrap support, and we set a nodal
243 support threshold of ≥70. We used Subset 7.3 gene trees without branch lengths to perform
244 independent runs (Table 1). These trees had one representative individual per subspecies/species.
245 We estimated specific numbers of reticulations (0, 1, 2, and 3) using maximum-likelihood
246 (*InferNetwork_ML*) in 50 runs, returning the five best networks. These analyses were optimized
247 after the search based on their branch lengths and inheritance probability. To obtain the best
248 representing number of reticulations, we assessed the log probabilities of the five best networks
249 of each run and calculated information criterion tests (AIC and BIC). These calculations were
250 performed according to Yu, Dong, Liu, & Nakhleh (2014). Networks were plotted with
251 Dendroscope v.3 (Huson & Scornavacca, 2012), in which branch lengths in coalescent units and
252 inheritance probabilities were shown. Finally, we summarized the five best networks
253 (*SummarizeNetworks* 5) using the major trees rule.

Introgression analysis

Given their recent and rapid radiation, as well as a possible reticulate evolution, we investigated patterns of introgression throughout bighorn and thinhorn genomes. Dfoil (Pease & Hahn, 2015), a D-statistics method, was employed by assuming a symmetric five-taxon phylogeny, which translates to having two in-group clades (P_1/P_2 *vs*. P_3/P_4) and an outgroup (O), where one in-group (P_1/P_2) is younger than the other (P_3/P_4). The test accounts for the presence and frequency of derived alleles in different taxon combinations, allowing the distinction between genealogical discordance driven by ILS and by introgression (Pease & Hahn, 2015). For all analyses, we considered a p-value cutoff of 0.01, and all other parameters were kept at default. We used all non-overlapping 100-kb GFs as input and reported all that were significant. The resulting significant introgression signals were summarized with *dfoil_analyze.py*, from which we obtained the total count per direction of gene flow (e.g., $P_1 \rightarrow P_3$). We ran an exhaustive analysis of all taxa combinations using the different thinhorn individuals as P_1 and P_2, and bighorn as P_3 and P_4 (Datasets 8-13: Figure S2-S7). The domestic sheep genome was used as an outgroup in all scenarios. To further study introgression patterns and narrow down possible adaptive genes, we estimated the asymmetric 4-taxon D-statistics (Green et al., 2010) in Dfoil. In this scenario, we used Dall as P_1 and Stone as P_2, followed by bighorn individuals as P_3, and the domestic sheep as the outgroup (Datasets 14-16: Figure S8). In contrast to the 5-taxon method, the resulting introgression signal represented bidirectional patterns ($P_1 \leftrightarrow P_3$; $P_2 \leftrightarrow P_3$). We obtained the total counts of significant introgression patterns.

The 4-taxon subset 14.6 GFs with the best mapping success genomes (one per subspecies/species; Table 1) and a given introgression signal (i.e., Dall or Stone↔bighorn) were

compared to the location of coat color, which were either complete or partially complete within their 100-kb GFs. These genes were obtained from literature review (Table S2) and the Kyoto Encyclopedia of Genes and Genomes (KEGG) melanogenesis pathway (humans: hsa04916; sheep: oas04916; reference pathway: ko04916) (Kanehisa, 2019; Kanehisa, Furumichi, Sato, Ishiguro-Watanabe, & Tanabe, 2020; Kanehisa, Sato, Furumichi, Morishima, & Tanabe, 2019). Gene descriptions were acquired from the NCBI database (https://www.ncbi.nlm.nih.gov/gene). Furthermore, we investigated the protein-protein interaction (PPI) networks per introgression pattern of coat color genes using string v.11.0 (Szklarczyk et al., 2015). This analysis illustrates whether the genes found within GFs with introgression signal code for proteins that interact. Quality filters were applied, including a high confidence threshold of 0.700, an FDR stringency of 1%, and we set the organism as *Ovis* spp. Cytoscape v.3.8.1 (Shannon et al., 2003) was used to improve visualization of the interaction networks. The genes with PPI and that directly interact were visualized as networks and color-coded based on the outputted pathway. We considered those pathways with strength higher than 2, which included 7 or more genes connected in the network. Additionally, we compared the GFs to the location of all other genes. If a gene was present in more than one type of introgression GF, we considered the window with at least 30-kb more inside its 100-kb interval. When genes were present within the entire 100-kb intervals of both introgression patterns, we excluded them. We compared the counts of either CDS or genes present in regions with and without introgression signal (Dall or Stone and bighorn separately) using a chi-squared test.

To ensure robust comparison and consistent introgression signal, we combined the 4-taxon Datasets 14-16 (Figure S8) (hereafter "4-taxon combined dataset") to narrow down the potential adaptive introgression patterns. Only windows in common between all datasets were

used, and we verified whether the introgression signal between Dall or Stone and bighorn would be lost by employing different individuals of the focal species. This dataset was compared to the selection analysis (see the "*Natural selection inference*" section), from which we obtained either complete or partially complete genes within their GFs. Gene descriptions were obtained from NCBI. We used the coding regions (CDS) found within the 4-taxon combined dataset to identify functional genes in biological processes using the PANTHER database v.14.0 with *Homo sapiens* as the model organism (Thomas et al., 2003; Mi et al., 2010; Mi, Muruganujan, Ebert, Huang, & Thomas, 2019; Mi et al., 2019). We also considered the function of some potentially introgressed genes not recognized by PANTHER (i.e., LOC plus gene number) as they are absent in *Homo sapiens*. We compared the presence of genes in regions with and without introgression signal in the 4-taxon combined dataset using a chi-squared test in the same way we did for the 4-taxon subset 14.6.

Natural selection inference

To infer the adaptive significance of potential introgression blocks, we extracted CDS from each genome using the domestic sheep genome coordinates using gffread (Pertea & Pertea, 2020). Extracted regions were verified using the reciprocal best hits method and the RefSeq CDS for the domestic sheep. Since all genomes were aligned to the domestic sheep and the same annotation file was used for CDS extraction, we were able to concatenate the CDS sequences for each gene as aligned sequences. These files were converted to *phylip* format prior to estimating per gene dN/dS ratios using a looped perl script (Hughes, 2011). We inferred natural selection patterns by employing CODEML in PAML (Yang, 2007) to estimate per CDS omega values (ω or dN/dS), which assessed the signals observed among the different lineages. The estimated ω

indicates whether the natural selection signal was negative/purifying ($\omega < 1$), neutral ($\omega = 1$), or positive ($\omega > 1$) (Yang, 2007). We set a threshold for each selection signal based on the observed distribution of ω (purifying: $\omega < 0.8$; neutral: $0.8 \leq \omega \leq 1.2$; positive: $\omega > 1.2$). We removed any CDS from the analysis with out-of-bounds values (ω: ≥ 5 and ≤ 0.0004; "OOB") to calculate the median ω per 100-kb window (same size of the introgression analyses) with R v4.0.2 (R Core Team, 2020) and Rstudio v1.3.1056 (RStudio Team, 2020). Results were visualized with the R package ggplot2.

Finally, we analyzed the selection patterns observed within blocks with introgression signals. We calculated the branch-site model in CODEML by employing two different topologies with either Dall or Stone as sister to bighorn (Figure 1e-f), which allowed us to calculate ω values for these specific branches (hereafter called "foreground"). Snow and the domestic sheep were considered background branches together with Dall or Stone depending on the topology being employed (Figure 1e-f). The likelihood ratio test (LRT) differentiates a null and an alternative hypothesis, where the former proposes either neutral or purifying selecting on foreground and background, while the latter demonstrates signals of positive selection in the foreground (Yang, 2007). We compared the resulting CDS ω ratios to the 4-taxon subset 14.6 and 4-taxon combined dataset, considering the introgression pattern observed within each GF (Dall or Stone↔bighorn). We used the LRT per CDS to calculate the p-value and false discovery rate (FDR) with the package pchisq (Becker, Chambers, & Wilks, 1988; Johnson, Kotz, & Balakrishan, 1994, 1995) and qvalue (Storey, Bass, Dabney, & Robinson, 2020) in r, respectively. We considered an alpha value of 0.05 with one as degree of freedom and 3.84 as the critical number.

Results

346 Whole-genome and population assessment

347 After mapping all bighorn, snow, and thinhorn sheep sequences against the domestic
348 sheep genome, the reconstructed repeat-masked genomes spanned on average a total of 47.9%
349 (Table S1). Most of these genomes had reasonable coverage throughout, ranging from 15-27.5X,
350 in which bighorn and thinhorn sheep had similar values, whereas snow sheep had the lowest
351 quantity of data mapped (Figure S1; Table S1). Additionally, we also mapped the goat genome,
352 which represented 47.7% after repeat-masking, with a 28.9X coverage (Figure S1k; Table S1).

353 Bighorn and thinhorn genomes demonstrated population structure, as the six bighorn
354 individuals clustered together and were well resolved from thinhorn sheep along PC axis 1
355 (Figure S9; Table S1). PC axis 2 separated Stone sheep from Dall sheep (Figure S9). Patterns of
356 nucleotide diversity varied among species (Before outlier test: 134,230 GFs; after: 119,343 GFs).
357 Autosomal diversity was significantly higher than the X chromosome in each species (p-
358 value<0.001) (Figure S10). Significant differences in diversity were found among species for all
359 chromosomes and autosomes with thinhorn exceeding bighorn (Figure S10a-b, d), whereas the X
360 chromosome diversity was significantly higher for bighorn than thinhorn (Figure S10c-d).

361

362 Speciation events through a phylogenomic perspective

363 Pachyceriform evolutionary history is characterized by multiple gene trees throughout
364 their genomes regardless of the dataset, GF and step size used (Figure 1d-f, S11; Table S3-S4).
365 After constraining, we observed that the accepted species tree (topology 1) was most prevalent,
366 followed by topologies 2-3 and 4-5 (Table S4). The topologies had variable nodal bootstrap
367 support, in which the species tree was the most supported, followed by topologies 2 and 3,
368 representing the relationship between Stone and bighorn (Table S5-S7). These values followed

the same pattern for all datasets used, even when using the goat as an outgroup (Table S5-S7). Moreover, the species tree was also prevalent under MSC in all datasets analyzed (Figure 1d, S12-S13). While using Datasets 2, 3 and 4 (with all individuals of each species), we observed the same topology when considering all chromosomes or only autosomes (Figure S12a). However, when considering only the X chromosome, individuals of each species had varying positions within their clades for the different GFs and step sizes (Figure S12b-g). The species trees observed for Datasets 5 to 6 (with fewer individuals per subspecies/species) were not variable for the different chromosomal partitions regardless of outgroup taxa (Figure S13a-c).

Given the species tree observed, we estimated the relative node ages and subsequently the divergence times of their speciation event (Figure 2a; Table S8). The relative node ages estimated for subsets 5.2 and 5.3 were robust and consistent for the different nodes (Table S8). From the relative node ages, we estimate that the thinhorn clade (Dall and Stone) speciated from bighorn at approximately 2.50 and 2.21 Ma for analyses done with 100-kb and 200-kb step sizes, respectively. This trio and snow sheep separated at around 2.85 and 2.63 Ma (Figure 2a). Looking further into bighorn and thinhorn divergence (GFs with 100-kb and 200-kb step size respectively: 10,758 and 6,207), Stone and bighorn were significantly less divergent than Dall and bighorn for all chromosomes and autosomes in the two subsets under Mann-Whitney U (Figure S14-S15a-b, d). The X chromosome had a similar pattern, though it was not significantly different (Figure S14-S15c-d). Additionally, the sister-species divergence (Figure S14-S15) was consistently higher than the intraspecific diversity (Figure S10).

Speciation mediated by ancient hybridization

Based on the different topologies observed for the phylogenomic inference (Figure 1d-f, S11; Table S4), we estimated a species network with distinct numbers of reticulation events (Figure S16-S19). We determined that three reticulation events demonstrated the best log probability and best fitted the models (AIC and BIC) (Table S9). When summarizing these reticulation networks, the most supported phylogeny was topology 1 (Figure 2a). We observed one reticulation event representing the origin of snow, and other two reticulations involved each with the origin of the trio (bighorn and thinhorn) and of Stone (from bighorn and Dall ancestors) (Figure 2b; S19).

To further investigate ancient hybridization patterns, we conducted the 5-taxon introgression analysis (Figure S2-S7). Most GFs showed a bidirectional relationship between the thinhorn lineage and a bighorn individual ($P_{1,2}\leftrightarrow P_3$ or $P_{1,2}\leftrightarrow P_4$) (Figure S20; Table S10-S11). When Stone sheep individuals were P_1 and P_2 (Datasets 8-10: Figure S20a; Table S10), the number of GFs with introgression signal from and into bighorn were similar. In contrast, when Dall and Stone individuals were P_1 and P_2 (Datasets 11-13: Figure S20b; Table S11), we observed that more GFs supported gene flow between Stone and bighorn. In this case, the direction of introgression was mostly from bighorn to Stone. This same pattern was observed in the 4-taxon D-statistics analysis (Datasets 14-16: Figure S21-S23), where a greater number of GFs supported the relationship between Stone and bighorn ($P_1\leftrightarrow P_3$) in all scenarios. The GF support was almost four times greater than that between Dall and bighorn ($P_2\leftrightarrow P_3$) (Figure S21-23), as observed in subset 14.6 with the best genomes (Figure 3a). By combining Datasets 14-16, we identified 80 GFs with signals between Dall and bighorn, and 333 between Stone and bighorn.

The GFs observed in subset 14.6 were compared to the coat color gene locations (Figure 3a-b; Table S12). We found 22 coat color genes in GFs with signals of introgression between Stone and bighorn sheep, and six such genes in GFs between bighorn and Dall sheep (Figure 3b). Based on the output from string for Stone and bighorn signals, 14 genes were directly part of the melanogenesis pathway (Table S13), but only seven interact directly (PPI p-value: 3.1E-10) (Figure 3c). The melanogenesis pathway had the highest number of coat color genes when considering genes not directly connected in the network, but other pathways were also observed and were related to various functions (Table S13). We identified an additional gene, *CALML6* (Figure 3b), that was not included in the string output, but is known to be in the human melanogenesis reference pathway (hsa04916). Moreover, two genes (*DTNBP1* and *HPS4*) were connected but involved in the biogenesis of lysosomal organelle complex (Figure 3b-c). There was no significant PPI enrichment (p-value: 1) for genes present within GFs with signals of Dall and bighorn. However, *TCF7L2* was directly involved in the melanogenesis pathway, and *AP1S1* and *CTNS* were part of the lysosome pathway (Figure 3b). The number of coat color genes present in regions with or without introgression signal between Dall or Stone and bighorn (Table S14-S15) did not differ significantly (Dall↔bighorn: $X^2_{(CDS)}$=2.0, p-value$_{(CDS)}$= 0.2; $X^2_{(genes)}$=0.1, p-value$_{(genes)}$= 0.8; Stone↔bighorn: $X^2_{(CDS)}$=1.7, p-value$_{(CDS)}$=0.2; $X^2_{(genes)}$=0.2, p-value$_{(genes)}$=0.7).

The genes present within the 4-taxon combined dataset (Figure S24; Table S16) were associated with multiple functions. Most functions were related to common biological processes, such as cell organization and metabolism (Figure S24). There were more genes present within GFs with introgression signal between Stone and bighorn (genes=324; CDS=531) than Dall and bighorn (genes=68; CDS=93) (Table S16). Furthermore, a gene within Stone and bighorn introgression signals was related to behavior (Figure S24b), as well as coat color genes within

436 GFs with introgression signal between Dall or Stone and bighorn (Figure 3b). Olfactory genes
437 were also observed in this combined dataset (Dall and bighorn: 11; Stone and bighorn: 17). Coat
438 color genes were observed at the same frequency in regions with or without introgression signal
439 between Dall and bighorn (Table S14-S15) (Dall↔bighorn: $X^2_{(CDS)}$=0.9, p-value$_{(CDS)}$= 0.4;
440 $X^2_{(genes)}$=2.4, p-value$_{(genes)}$= 0.1). We observed a trend in which coat color CDS/genes within GFs
441 with introgression signal between Stone and bighorn were more present than would be expected
442 by chance (Table S15); however, only one such comparison was significant (Stone↔bighorn:
443 $X^2_{(CDS)}$=43.5, p-value$_{(CDS)}$=4.3E-11).
444
445 Potential adaptive introgression
446 Given the ancient hybridization patterns observed between Dall or Stone and bighorn, we
447 also observed distinct selection signals throughout their genomes. We used the distribution of ω
448 to set a threshold for each selection signal (Figure S25). After filtering CDS based on OOB or
449 insufficient genomic information, we observed 19,151 CDS in the one ratio analysis. Throughout
450 Dataset 7 genomes (one individual per subspecies/species), most CDS within bins underwent
451 purifying selection (89.64%; mean ω = 0.19), followed by neutral (7.53%; mean ω = 0.96) and
452 positive signals (2.83%; mean ω = 1.86) (Figure 4). When considering only bins containing coat
453 color CDS, we observed mostly purifying signals (93.3%; mean ω = 0.15), followed by positive
454 (4.2%; mean ω = 1.65) and neutral (2.5%; mean ω = 0.98) selection. The distribution of median
455 ω per 100-kb window showed a consistent pattern over all chromosomes (Figure 4). Furthermore,
456 when employing the branch-site model, we failed to reject the null hypothesis in most CDS
457 (Table S12, S16) and observed no positive selection in the coat color genes within Subset 14.6

458 (Table S12). Only one gene underwent positive selection in the 4-taxon combined dataset (Table
459 S16).
460
461 **Discussion**
462 Evolutionary history of Pachyceriforms
463 By analyzing multiple whole-genome sequences, we confirmed the species tree of the
464 Pachyceriform clade, the topology seen previously by employing different molecular markers
465 (e.g., Bunch et al., 2006; Dotsev et al., 2019; Rezaei et al., 2010). We observed a clear species
466 delimitation of bighorn and thinhorn sheep (Figure S12-S13; Table S4), including subspecies
467 distinction of the latter. Concomitantly, we observed that π (Figure S10) of each species was
468 lower than the divergence level between them (Figure S14-S15). Moreover, this was also
469 confirmed by reconstruction under MSC, where regardless of how many individuals were used,
470 the species tree was still recovered (Figure S12). The main variation in this species tree topology
471 was the movement of bighorn or thinhorn individuals within their respective clades when
472 considering GF and step sizes on the X chromosome (Figure S12b-g). Their different collection
473 sites as well as mapping success could have impacted their positions (Table S1).
474 While demonstrating a robust species tree signal, we also observed distinct genealogical
475 discordance patterns throughout their genomes (Table S4). These conflicting signals were
476 possibly due to their recent and rapid radiation (Figure 2a; Table S8), which could have retained
477 signals of ILS and ancient hybridization (Degnan & Rosenberg, 2009). These gene trees
478 presented high topological movement of snow sheep in the different datasets and partitions
479 (Table S4). Genome quality and coverage plays an important role in how the phylogenies are
480 estimated (Young & Gillung, 2019), and the different topological positions of snow sheep could

be due to its lower genome coverage (Table S1). More snow sheep genomes are needed to fully understand its role in the speciation of this group. Additionally, there were no major topological differences when using either the domestic sheep (Dataset 5) or goat (Dataset 6) as the outgroup (Table S4). Thus, the genealogical discordance observed was not caused or affected by outgroup biases.

Moreover, even when the topologies were constrained to remove potential biases, we still observed conflicting signals that placed Dall or Stone as sister to bighorn (Table S3-S4). These topologies varied in bootstrap support, where the topology 1 (known "species tree") was the most supported, followed by topologies 2-3 (Stone and bighorn) and 4-5 (Dall and bighorn) (Table S5-S7). We observed lower support for some phylogenomic relationships (Table S5-S7), which could be due to genome mapping success, as well as to the lower π (Figure S10) and divergence (Figure S14-S15) within and between species, respectively. A certain number of informative sites are needed to maintain higher bootstrap values (Soltis & Soltis, 2003), and sequences of closely related species, such as bighorn and thinhorn, can generate lower phylogenomic support. The low π was also characterized by significant differences between thinhorn and bighorn on the all chromosomes and autosomes (Figure S10a-b, d). The bighorn individuals were mostly from regions with intraspecific admixture (Hogg et al., 2006; Miller et al., 2014; Miller et al., 2012), which could explain the pattern observed. On the X chromosome, however, we observed that π was significantly higher in bighorn (Figure S10c-d). Additionally, the X chromosome of both bighorn and thinhorn was less diverse than the autosomes (Figure S10). Some studies have observed that the X chromosome presents lower recombination rates, which can decrease the genetic variability of species when compared to the rest of the genome (Edelman et al., 2019; Figueiro et al., 2017; Li et al., 2019). Another explanation is that there are fewer copies of the X

chromosome when compared to autosomes. When assuming sex-specific Ne equivalent, we can therefore consider the Ne on the X chromosome as only 0.75 beta of the autosomes (Kardos et al., 2015; Hammer et al., 2008; Hedrick, & Parker 1997).

The significant difference between d_{xy} values (Dall and bighorn *vs*. Stone and bighorn) also supported the gene trees observed, specifically those estimated with more GFs (Figure S14). The relationship between Stone and bighorn was more prevalent throughout the genomes when compared to Dall and bighorn, and they were less divergent than Dall and bighorn, which also agrees with previous studies (Loehr et al., 2006, 2008; Hoefs & Bunch, 2001). There were no significant differences on the X chromosome (with 100 or 200-kb step size), which is potentially generated by lower recombination rates and number of copies as described previously. These patterns may have been driven by ancient hybridization with potential genomic incorporation between Stone and bighorn. The less extensive Dall and bighorn introgression signals would be potentially due to the presence of ILS or other phenomena, such as natural selection, as it was less common and less supported in the different datasets, GF and step sizes used. Incongruent signals, such as ILS, are randomly placed throughout the genome (Degnan & Rosenberg, 2009; Payseur & Rieseberg, 2016), which might not have affected the nucleotide divergence estimates of Dall and bighorn, resulting in higher divergence between them.

Ancient hybridization and its adaptive consequences

Given the genealogical discordance we observed from vertical transmission, we investigated whether Pachyceriform speciation underwent reticulate evolution. We detected at least three possible reticulation events (Table S9). Therefore, it is extremely important to consider ILS and hybridization events in phylogenomic inferences when dealing with recent speciation, as

has been demonstrated for bears (Kumar et al., 2017). PhyloNet provides a consistent recovery of the "true" species tree under high levels of gene flow events (Solís-Lemus, Yang & Ané, 2016), and enabled us to summarize the best log probability reticulate networks, which resulted in topology 1 (species tree: Figure 2a). By analyzing the best network (Figure 2b; Table S9), we observed that snow sheep might have an important role to how bighorn and thinhorn originated; however, more individuals are needed to further evaluate this relationship. Here we considered all gene trees of subsets 7.3, including those where snow sheep moved between branches (N=6,780), since it would be arbitrary to remove these phylogenies, and we tried to compensate by applying a bootstrap threshold. Lower quality sequences could impact the reticulations observed (Cao, Liu, Ogilvie, Yan, & Nakhleh, 2019), although most of the genomes used in this study were of reasonable sequence coverage and quality (Figure S1; Table S1).

Furthermore, bighorn and thinhorn originated from at least one reticulation event (Figure 2b). We also observed a signal placing Stone as having originated from Dall and bighorn's ancestor, with more contribution from Dall (71%) (Figure 2b), which agrees with the π, d_{xy}, and introgression results (Figure S10; S14-S15; S20-S23). These networks demonstrate a complex mosaic of events that took place and gave rise to today's known bighorn and thinhorn species. They could have had a hybrid speciation, and not just hybridization events (Cao et al., 2019). The ancient hybridization event(s) between Stone and bighorn has also been detected using conventional genetic markers (e.g., Loehr et al., 2006, 2008; Meadows et al., 2006; Worley et al., 2004).

We have improved our understanding of these ancient event(s) by analyzing multiple bighorn and thinhorn individuals to identify potential introgression signatures within their genomes. Most of the introgression signals observed for the 5-taxon analyses were bidirectional

between the lineage of thinhorn and bighorn (Figure S20; Table S10-S11). This pattern was observed regardless of using only Stone as P_1/P_2 or Dall and Stone as P_1 and P_2, respectively, which could mean that a ghost lineage might be crucial in interpreting these results (Pease & Hahn, 2015). Hybridization might have happened between a ghost lineage ancestral to bighorn and Dall, followed by further hybridization between bighorn and the lineage leading to Stone sheep. When we compared using only Stone as P_1/P_2 (Figure S20a) to using Dall and Stone as P_1 and P_2 (Figure S20b), the number of windows from bighorn to Stone increased when both Dall and Stone were used. This observation, and their lower divergence patterns (Figure S14-S15), confirm more recent admixture between Stone and bighorn.

Although the 5-taxon results were robust across all possible combinations, using two bighorn individuals per analysis could generate biases since these individuals had distinct population histories (Coltman et al., 2002; Miller et al., 2014, 2012). Therefore, we decided to further investigate their introgression patterns by employing an asymmetric analysis, where only one bighorn individual per subset was used (Figure S8). Even then, we observed the same signal as the 5-taxon analyses, where there were more signals between Stone and bighorn (Figure 3a; Figure S21-S23). When we compared all datasets ("4-taxon combined dataset"), we observed fewer signal, which could be explained by genetic drift of these neutral introgression blocks (Burgarella et al., 2019). However, by only keeping those in common between introgression patterns, we were able to retrieve a more robust introgression signal between these species, which retained a stronger bidirectional relationship between Stone and bighorn. Moreover, based on all comparisons done, there were more genes present within GFs with introgression signal between Stone and bighorn (Table S12, S14). These GFs included potentially functional coat color genes.

572 Coat color genes observed in GFs with introgression signal were mostly related to the
573 melanogenesis pathway, although other functional pathways were also observed (Figure 3b-c;
574 Table S12-S14). All analyzed GFs within subset 14.6 and the 4-taxon combined dataset
575 demonstrated a strong purifying signal throughout the different chromosomes when considering
576 an ω per gene among species (Figure 4). Purifying selection removes deleterious alleles,
577 maintaining proper gene function (Charlesworth, 1993), and this pattern was associated with
578 lower genetic diversity (Figure S10) and potentially caused by background selection (Branca et
579 al., 2011; Comeron, 2017; Cvijovic, Good, & Desai, 2018; Talla et al., 2019). When analyzing
580 the branch-site model, coat color genes observed in the D-statistics GFs were mostly under either
581 neutral or purifying selection, and some of them have key roles in how pigment is produced and
582 distributed (Figure 3b; Table S12, S14). Most of these genes were found within Stone and
583 bighorn windows, which demonstrates that these blocks could have been incorporated, and their
584 functions retained. This is consistent with enriched coat color CDS present in GFs with
585 introgression signal between Stone and bighorn (Table S15). For example, the gene *CALML6*
586 found within Stone and bighorn has roles in the melanogenesis pathway, as well as olfaction
587 (Ramos-Lopez et al., 2019).

588 We observed several genes related to olfactory functions in sheep which were under
589 neutral or purifying selection (Table S16). Thus, the function of *CALML6* may be maintained by
590 selection as it is linked to multiple biologically important traits. We also observed genes related
591 to the lysosomal organelle complex (*HPS4* and *DTNBP1*: Figure 3b-c), and mutations in this
592 complex lead to diseases in humans (Sitaram & Marks, 2012; Serre, Busuttil, & Botto, 2018).
593 Most genes present within these genomic blocks with introgression signals were related to trivial
594 biological functions, but we also observed a behavior-related gene (Table S16). Deficit in

595 *SHANK2* generates reduced social interaction, and impaired spatial learning (Won et al., 2012).
596 Darker coat color can be potentially associated with social dominance and mating behavior in
597 sheep (Loehr et al., 2008), and *SHANK2* might contribute to variation in these characteristics.
598 Moreover, almost all CDS within Stone and bighorn GFs demonstrated no positive selection
599 (Table S12, S14), and the one gene that exhibited positive selection (Table S16) lacked functional
600 annotation (https://www.ncbi.nlm.nih.gov/gene/286464). Considering the higher presence of
601 purifying selection among lineages (Figure 4), as well as the failure to reject the branch-site
602 model null hypothesis of either neutral or purifying signals in most genes, it is possible that
603 introgression between Stone and bighorn maintained a dark coat color genetic architecture
604 already present rather than re-introducing it.

605 In contrast, the GFs with introgression signal between Dall and bighorn contained
606 relatively few coat color genes, and those that were present did not interact directly (Figure 3b;
607 Table S12). In the 4-taxon combined dataset we observed only two genes within these GFs,
608 neither of which displayed positive selection. One gene (*CCN1*) is involved in pro-inflammatory
609 functions in the skin and stimulated by UVB to maintain normal epidermal melanocyte (Henrot,
610 Truchetet, Fisher, Taïeb, & Cario, 2018; Xu et al., 2018), whereas the (*CTNS*) is related to
611 melanin synthesis (Chiaverini et al., 2012) and controls the presence of a negative regulator of
612 this pathway (Sturm, 2012). Within these GFs, we also observed olfactory-related genes (Table
613 S15); however, no genes related to behavior were found.

614 Moreover, the lack of positive selection could be associated to the type of selective
615 pressure. When hard sweeps are present, stronger selection effects are observed, in which π
616 decreases, making inference of selection from these regions better to detect (Burgarella et al.,
617 2019). However, other signals can be difficult to detect, such as soft sweeps, which maintain π

with no drastic changes around these regions (Harris, Sackman, & Jensen, 2018). Both types of sweeps can be present in introgression regions and contribute to adaptive introgression (Burgarella et al., 2019). Although the branch-site model is a great tool to detect selection, it can become overwhelmed by the saturation of dS, leading to higher false-negatives (Gharib & Robinson-Rechavi, 2013), and lose detection power at low divergence regions (Yang & dos Reis, 2010).

Genome-wide evolutionary aspects

Our results with different window and step sizes demonstrate a complex network of events and confirm that distinct parts of the genome present different evolutionary histories. Such patterns have been demonstrated for various groups, e.g., butterflies (Martin et al., 2016), bears (Kumar et al., 2017), cats (Figueiro et al., 2017; Li et al., 2019) and mosquitoes (Fontaine et al., 2015). With smaller window sizes we more accurately infer speciation by having GFs with more specific recombination rates, and not just great genomic blocks with various rates. High and low recombination rates play an important role in detecting the "true" phylogeny and the presence of introgression patterns, since the former are diminished under lower rates (Edelman et al., 2019). Thus, the importance of evaluating and applying different sizes to determine the evolutionary history of species, specifically of those with recent and rapid radiation.

Concluding remarks

Stone and bighorn present clear evidence of ancient hybridization throughout their genomes, with a stronger signal between Stone and bighorn, and a less divergent relationship than between Dall and bighorn. This ancient hybridization left distinct introgression patterns

641 throughout Stone and bighorn genomes, such as genes related to coat color and behavior, which
642 may have implications for how Stone sheep developed/maintained their distinct pelage. Through
643 gene flow, genomic blocks were incorporated into Stone individuals leading to their dark
644 coloration, whereas in the absence of such introgression Dall maintained its white coat pattern.
645 Alternatively, the ancestral Pachyceriforms may have exhibited a darker coat color, and the white
646 coat of Dall is subsequent adaptation to northern environments. The Pachyceriform clade is
647 thought to have evolved from either an Ammon- or Nivicola-like individual, both of which
648 theoretically have darker coat color (Bunch et al., 2006; Cowan, 1940).

649 In contrast, the signals of hybridization obtained between Dall and bighorn were less
650 apparent and more random. The genealogical discordance patterns observed between Dall and
651 bighorn could have been caused by multiple mechanisms. First, Stone sheep may have been a
652 vector for blocks from bighorn as a result of secondary contact with Dall following the ice retreat,
653 given the wide separation between the geographic ranges of Dall and bighorn (Klein, 1965; Loehr
654 et al., 2006, 2008). A similar process has been proposed for bears (Kumar et al., 2017), in which
655 the geographically wide-spread grizzly bear would have been the vector species between polar or
656 American black bear and Asiatic black bear. Another possibility would be that other phenomena
657 generated incongruent signals throughout Dall's genome, such as ILS and natural selection.

658

659 **Acknowledgements**

660 This study was financially supported by grants from the National Key Research and
661 Development Program-Key Projects of International Innovation Cooperation between
662 Governments (2017YFE0117900), the External Cooperation Program of Chinese Academy of
663 Sciences (152111KYSB20190027) and a Natural Sciences and Engineering Research Council of

Canada Discovery Grant to DWC. We are grateful to the hunters, outfitters and biologists who provided specimens for whole genome sequencing. We also thank Marty Kardos and two anonymous reviewers for their constructive comments and feedback.

References

Andrews, S. (2019, January). *FastQC: a quality control tool for high throughput sequence data* [Software]. Retrieved from https://www.bioinformatics.babraham.ac.uk/projects/fastqc/

Barlow, A., Cahill, J. A., Hartmann, S., Theunert, C., Xenikoudakis, G., Fortes, G. G., ... Hofreiter, M. (2018). Partial genomic survival of cave bears in living brown bears. *Nature Ecology and Evolution*, *2*(10), 1563–1570. doi: https://doi.org/10.1038/s41559-018-0654-8

Becker, R. A., Chambers, J. M., & Wilks, A. R. (1988). The new S language. Wadsworth & Brooks/Cole.

Bolger, A. M., Lohse, M., Usadel, B. (2014) Trimmomatic: A flexible trimmer for Illumina Sequence Data. *Bioinformatics*, *30*(15), 2114–2120. doi: https://doi.org/10.1093/bioinformatics/btu170

Branca, A., Paape, T. D., Zhou, P., Briskine, R., Farmer, A. D., Mudge, J., … Tiffin, P. (2011). Whole-genome nucleotide diversity, recombination, and linkage disequilibrium in the model legume Medicago truncatula. *Proceedings of the National Academy of Sciences of the United States of America*, *108*(42). doi: https://doi.org/10.1073/pnas.1104032108

Bravo, G. A., Antonelli, A., Bacon, C. D., Bartoszek, K., Blom, M. P. K., Huynh, S., ... Edwards, S. V. (2019). Embracing heterogeneity: Coalescing the tree of life and the future of phylogenomics. *PeerJ*, *2019*(2), 1–60. doi: https://doi.org/10.7717/peerj.6399

Bunch, T. D., Wu, C., Zhang, Y. P., & Wang, S. (2006). Phylogenetic analysis of snow sheep (Ovis nivicola) and closely related taxa. *Journal of Heredity*, *97*(1), 21–30. doi: https://doi.org/10.1093/jhered/esi127

Burgarella, C., Barnaud, A., Kane, N. A., Jankowski, F., Scarcelli, N., Billot, C., ... Berthouly-Salazar, C. (2019). Adaptive introgression: An untapped evolutionary mechanism for crop adaptation. *Frontiers in Plant Science*, *10*, 1–17. doi: https://doi.org/10.3389/fpls.2019.00004

Bushnell, B. (2020, October). *BBMap: BBMap short read aligner, and other bioinformatic tools.* [Software]. Retrieved from https://sourceforge.net/projects/bbmap/

Cao, Z., Liu, X., Ogilvie, H. A., Yan, Z., & Nakhleh, L. (2019). Practical aspects of phylogenetic network analysis using PhyloNet. *BioRxiv*. doi: https://doi.org/10.1101/746362

Capella-Gutiérrez, S., Silla-Martínez, J. M., & Gabaldón, T. (2009). trimAl: A tool for automated alignment trimming in large-scale phylogenetic analyses. *Bioinformatics*, *25*(15), 1972–1973. doi: https://doi.org/10.1093/bioinformatics/btp348

Chang, C. C., Chow, C. C., Tellier, L. C. A. M., Vattikuti, S., Purcell, S. M., & Lee, J. J. (2015). Second-generation PLINK: Rising to the challenge of larger and richer datasets. *GigaScience*, *4*(1), 1–16. doi: https://doi.org/10.1186/s13742-015-0047-8

Charlesworth, B. (2012). The effects of deleterious mutations on evolution at linked sites. *Genetics*, *190*(1), 5–22. doi: https://doi.org/10.1534/genetics.111.134288

Chiaverini, C., Sillard, L., Flori, E., Ito, S., Briganti, S., Wakamatsu, K., ... Ballotti, R. (2012). Cystinosin is a melanosomal protein that regulates melanin synthesis. *The FASEB Journal*, *26*(9), 3779–3789. doi: https://doi.org/10.1096/fj.11-201376

Cieslak, M., Reissmann, M., Hofreiter, M., & Ludwig, A. (2011). Colours of domestication. *Biological Reviews*, *86*(4), 885–899. doi: https://doi.org/10.1111/j.1469-185X.2011.00177.x

Coltman, D. W., Festa-Bianchet, M., Jorgenson, J. T., & Strobeck, C. (2002). Age-dependent sexual selection in bighorn rams. *Proceedings of the Royal Society B: Biological Sciences*, *269*(1487), 165–172. doi: https://doi.org/10.1098/rspb.2001.1851

Comeron, J. M. (2017). Background selection as null hypothesis in population genomics: Insights and challenges from drosophila studies. *Philosophical Transactions of the Royal Society B: Biological Sciences*, *372*(1736). https://doi.org/10.1098/rstb.2016.0471

Cowan, I. M. (1940). Distribution and Variation in the Native Sheep of North America. American Midland Naturalist, 24(3), 505. doi: https://doi.org/10.2307/2420858

Cvijović, I., Good, B. H., & Desai, M. M. (2018). The effect of strong purifying selection on genetic diversity. *Genetics*, *209*(4), 1235–1278. doi: https://doi.org/10.1534/genetics.118.301058

De Mita, S., & Siol, M. (2012). EggLib: Processing, analysis and simulation tools for population genetics and genomics. *BMC Genetics*, *13*(1), 27. doi: https://doi.org/10.1186/1471-2156-13-27

Degnan, J. H., & Rosenberg, N. A. (2009). Gene tree discordance, phylogenetic inference and the multispecies coalescent. *Trends in Ecology and Evolution*, *24*(6), 332–340. doi: https://doi.org/10.1016/j.tree.2009.01.009

Deng, J., Xie, X. L., Wang, D. F., Zhao, C., Lv, F. H., Li, X., Yang, J., ... Li, M. H. (2020). Paternal Origins and Migratory Episodes of Domestic Sheep. *Current Biology*, *30*(20), 4085-4095.e6. doi: https://doi.org/10.1016/j.cub.2020.07.077

D'Mello, S. A. N., Finlay, G. J., Baguley, B. C., & Askarian-Amiri, M. E. (2016). Signaling pathways in melanogenesis. *International Journal of Molecular Sciences*, *17*(7), 1–18. doi: https://doi.org/10.3390/ijms17071144

Dotsev, A. V., Kunz, E., Shakhin, A. V., Petrov, S. N., Kostyunina, O. V., Okhlopkov, ... Zinovieva, N. A. (2019). The first complete mitochondrial genomes of snow sheep (Ovis nivicola) and thinhorn sheep (*Ovis dalli*) and their phylogenetic implications for the genus Ovis. *Mitochondrial DNA Part B: Resources*, *4*(1), 1332–1333. doi: https://doi.org/10.1080/23802359.2018.1535849

Edelman, N. B., Frandsen, P. B., Miyagi, M., Clavijo, B., Davey, J., Dikow, R. B., ... Patterson, N. (2019). Butterfly radiation. *Science*, *599*, 594–599.

Ekblom, R., & Wolf, J. B. W. (2014). A field guide to whole-genome sequencing, assembly and annotation. *Evolutionary Applications*, *7*(9), 1026–1042. https://doi.org/10.1111/eva.12178

Fan, R., Xie, J., Bai, J., Wang, H., Tian, X., Bai, R., ... Dong, C. (2013). Skin transcriptome profiles associated with coat color in sheep. *BMC Genomics*, *14*(1). doi: https://doi.org/10.1186/1471-2164-14-389

Feulner, P. G. D., Gratten, J., Kijas, J. W., Visscher, P. M., Pemberton, J. M., & Slate, J. (2013). Introgression and the fate of domesticated genes in a wild mammal population. *Molecular Ecology*, *22*(16), 4210–4221. doi: https://doi.org/10.1111/mec.12378

Festa-Bianchet, M. (2020a). *Ovis canadensis. The IUCN Red List of Threatened Species 2020*, e.T15735A22146699. doi: https://dx.doi.org/10.2305/IUCN.UK.2020-2.RLTS.T15735A22146699.en. Downloaded in April 2021.

Festa-Bianchet, M. (2020b). *Ovis dalli*. *The IUCN Red List of Threatened Species 2020*, e.T39250A22149895. doi: https://dx.doi.org/10.2305/IUCN.UK.2020-2.RLTS.T39250A22149895.en. Downloaded in April 2021.

Figueiro, H.V. (2019, June). *Introgression-penguins* [Source code]. Retrieved from https://github.com/henriquevf/Introgression-penguins

Figueiró, H. V., Li, G., Trindade, F. J., Assis, J., Pais, F., Fernandes, G., ... Eizirik, E. (2017). Genome-wide signatures of complex introgression and adaptive evolution in the big cats. *Science Advances*, *3*(7), 1–14. doi: https://doi.org/10.1126/sciadv.1700299

Flouri, T., Jiao, X., Rannala, B., & Yang, Z. (2018). Species tree inference with BPP using genomic sequences and the multispecies coalescent. *Molecular Biology and Evolution*, *35*(10), 2585–2593. doi: https://doi.org/10.1093/molbev/msy147

Fontaine, M. C., Pease, J. B., Steele, A., Waterhouse, R. M., Neafsey, D. E., Sharakhov, I. V., ... Besansky, N. J. (2015). Extensive introgression in a malaria vector species complex revealed by phylogenomics. *Science*, *347*(6217), 1258524. doi: https://doi.org/10.1126/science.1258524

Geist, V. (1971). *Mountain sheep. A study in behavior and evolution*. Chicago and London: University of Chicago Press.

Gharib, W., Robinson-Rechavi, M. (2013). The branch-site test of positive selection is surprisingly robust but lacks power under synonymous substitution saturation and variation in gc. Molecular Biology and Evolution, 30(7), 1675–1686. doi: https://doi.org/10.1093/molbev/mst062

Gratten, J., Pilkington, J. G., Brown, E. A., Beraldi, D., Pemberton, J. M., & Slate, J. (2010). The genetic basis of recessive self-colour pattern in a wild sheep population. *Heredity*, *104*(2), 206–214. doi: https://doi.org/10.1038/hdy.2009.105

Hammer, M. F., Mendez, F. L., Cox, M. P., Woerner, A. E., Wall, J. D. (2008). Sex-biased evolutionary forces shape genomic patterns of human diversity. *PLoS Genetics*, *4*(9), e1000202. doi: https://doi.org/10.1371/journal.pgen.1000202

Harris, M. L., Baxter, L. L., Loftus, S. K., & Pavan, W. J. (2010). Sox proteins in melanocyte development and melanoma. *Pigment Cell and Melanoma Research*, *23*(4), 496–513. doi: https://doi.org/10.1111/j.1755-148X.2010.00711.x

Harris, R. B., Sackman, A., Jensen, J. D. (2018). On the unfounded enthusiasm for soft selective sweeps II: Examining recent evidence from humans, flies, and viruses. PLOS Genetics, 14(12), e1007859. doi: https://doi.org/10.1371/journal.pgen.1007859

Hedrick, P. W. (2013). Adaptive introgression in animals: Examples and comparison to new mutation and standing variation as sources of adaptive variation. *Molecular Ecology*, *22*(18), 4606–4618. doi: https://doi.org/10.1111/mec.12415

Hedrick, P. W., Parker, J. D. (1997). Evolutionary genetics and genetic variation of haplodiploids and x-linked genes. *Annual Review of Ecology and Systematics*, *28*, 55–83. doi: https://doi.org/10.1146/annurev.ecolsys.28.1.55

Henrot, P., Truchetet, M. E., Fisher, G., Taïeb, A., & Cario, M. (2018). CCN proteins as potential actionable targets in scleroderma. *Experimental Dermatology*, *28*(1), 11–18. doi: https://doi.org/10.1111/exd.13806

Hiendleder, S., Kaupe, B., Wassmuth, R., & Janke, A. (2002). Molecular analysis of wild and domestic sheep questions current nomenclature and provides evidence for domestication from two different subspecies. *Proceedings of the Royal Society B: Biological Sciences*, *269*(1494), 893–904. doi: https://doi.org/10.1098/rspb.2002.1975

Hoefs, M., & Bunch, T. D. (2001). Lumpy jaw in wild sheep and its evolutionary implications. *Journal of Wildlife Diseases*, *37*(1), 39–48. doi: https://doi.org/10.7589/0090-3558-37.1.39

Hogg, J. T., Forbes, S. H., Steele, B. M., & Luikart, G. (2006). Genetic rescue of an insular population of large mammals. *Proceedings of the Royal Society B: Biological Sciences*, 273(1593), 1491–1499. doi: https://doi.org/10.1098/rspb.2006.3477

Hu, X. J., Yang, J., Xie, X. L., Lv, F. H., Cao, Y. H., Li, W. R., ... Li, M. H. (2018). The genome landscape of Tibetan sheep reveals adaptive introgression from Argali and the history of early human settlements on the Qinghai-Tibetan Plateau. *Molecular Biology and Evolution*, *36*(2), 283–303. doi: https://doi.org/10.1093/molbev/msy208

Hughes, J. (2011, October). *Sequence-manipulation/Fasta2Phylip.pl* [Source code]. Retrieved from https://github.com/josephhughes/Sequence-manipulation/blob/master/Fasta2Phylip.pl

Huson, D. H., Scornavacca, C. (2012). Dendroscope 3: an interactive tool for rooted phylogenetic trees and networks. Systematic Biology, 61(6), 1061–1067. doi: https://doi.org/10.1093/sysbio/sys062

IBM Corp. (2020). *IBM SPSS Statistics for Windows, Version 27.0* [Software]. Armonk, NY: IBM Corp. Retrieved from https://www.ibm.com/ca-en

Jackson, E., Heidl, M., Imfeld, D., Meeus, L., Schuetz, R., & Campiche, R. (2019). Discovery of a highly selective MC1R agonists pentapeptide to be used as a skin pigmentation enhancer and with potential anti-aging properties. *International Journal of Molecular Sciences*, *20*(24), 1–16. doi: https://doi.org/10.3390/ijms20246143

Johnson, N. L., Balakrishnan, N., & Kotz, S. (1994). *Continuous univariate distributions* (2nd ed., Vol. 1). New York: John Wiley & Sons.

Johnson, N. L., Balakrishnan, N., & Kotz, S. (1995). *Continuous univariate distributions* (2nd ed., Vol. 2). New York: John Wiley & Sons.

Junier, T., & Zdobnov, E. M. (2010). The Newick utilities: high-throughput phylogenetic tree processing in the UNIX shell. *Bioinformatics*, *26*(13), 1669–1670. doi: https://doi.org/10.1093/bioinformatics/btq243

Kanehisa, M. (2019). Toward understanding the origin and evolution of cellular organisms. *Protein Science*, *28*(11), 1947–1951. doi: https://doi.org/10.1002/pro.3715

Kanehisa, M., Furumichi, M., Sato, Y., Ishiguro-Watanabe, M., & Tanabe, M. (2020). KEGG: integrating viruses and cellular organisms. *Nucleic Acids Research*, 1–7. doi: https://doi.org/10.1093/nar/gkaa970

Kanehisa, M., Sato, Y., Furumichi, M., Morishima, K., & Tanabe, M. (2019). New approach for understanding genome variations in KEGG. *Nucleic Acids Research*, *47*(D1), D590–D595. doi: https://doi.org/10.1093/nar/gky962

Kardos, M., Luikart, G., Allendorf, F. W. (2015). Measuring individual inbreeding in the age of genomics: marker-based measures are better than pedigrees. *Heredity*, *115*, 63–72. doi: https://doi.org/10.1038/hdy.2015.17

Kijas, J. W., Porto-Neto, L., Dominik, S., Reverter, A., Bunch, R., McCulloch, R., ... the International Sheep Genomics Consortium. (2014). Linkage disequilibrium over short

physical distances measured in sheep using a high-density SNP chip. *Animal Genetics*, *45*(5), 754–757. doi: https://doi-org.login.ezproxy.library.ualberta.ca/10.1111/age.12197

Klein, D. R. (1965). Postglacial Distribution Patterns of Mammals in the Southern Coastal Regions of Alaska. *Arctic*, *18*(1), 7. doi: https://doi.org/10.14430/arctic3446

Kobayashi, Y., Mizusawa, K., Saito, Y., & Takahashi, A. (2012). Melanocortin systems on pigment dispersion in fish chromatophores. *Frontiers in Endocrinology*, *3*, 1–6. doi: https://doi.org/10.3389/fendo.2012.00009

Korneliussen, T. S., Albrechtsen, A., & Nielsen, R. (2014). ANGSD: Analysis of Next Generation Sequencing Data. *BMC Bioinformatics*, *15*(1), 1–13. doi: https://doi.org/10.1186/s12859-014-0356-4

Koseniuk, A., Ropka-Molik, K., Rubiś, D., & Smołucha, G. (2018). Genetic background of coat colour in sheep. *Archives Animal Breeding*, *61*(2), 173–178. doi: https://doi.org/10.5194/aab-61-173-2018

Kulski, J. K. (2016). Next-Generation Sequencing — An Overview of the History, Tools, and "Omic" Applications. In *Next Generation Sequencing - Advances, Applications and Challenges* (Issue tourism, p. 13). InTech. doi: https://doi.org/10.5772/61964

Kumar, V., Lammers, F., Bidon, T., Pfenninger, M., Kolter, L., Nilsson, M. A., & Janke, A. (2017). The evolutionary history of bears is characterized by gene flow across species. *Scientific Reports*, *7*(April), 1–10. doi: https://doi.org/10.1038/srep46487

Li, G., Figueiró, H. V., Eizirik, E., Murphy, W. J. (2019a). Recombination-Aware Phylogenomics Reveals the Structured Genomic Landscape of Hybridizing Cat Species. *Molecular Biology and Evolution*, *36*(10), 2111–2126. doi: https://doi.org/10.1093/molbev/msz139

Li, C., Nguyen, V., Clark, K. N., Zahed, T., Sharkas, S., Filipp, F. V., & Boiko, A. D. (2019b). Down-regulation of FZD3 receptor suppresses growth and metastasis of human melanoma independently of canonical WNT signaling. *Proceedings of the National Academy of Sciences of the United States of America*, *116*(10), 4548–4557. doi: https://doi.org/10.1073/pnas.1813802116

Li, H., & Durbin, R. (2009). Fast and accurate short read alignment with Burrows-Wheeler transform. *Bioinformatics*, *25*(14), 1754–1760. doi: https://doi.org/10.1093/bioinformatics/btp324

Li, H., Handsaker, B., Wysoker, A., Fennell, T., Ruan, J., Homer, N., ... Durbin, R. (2009). The Sequence Alignment/Map format and SAMtools. *Bioinformatics*, *25*(16), 2078–2079. doi: https://doi.org/10.1093/bioinformatics/btp352

Loehr, J., Carey, J., Ylönen, H., & Suhonen, J. (2008). Coat darkness is associated with social dominance and mating behavior in a mountain sheep hybrid lineage. *Animal Behaviour*, *76*(5), 1545–1553. doi: https://doi.org/10.1016/j.anbehav.2008.07.012

Loehr, J., Worley, K., Grapputo, A., Carey, J., Veitch, A., & Coltman, D. W. (2006). Evidence for cryptic glacial refugia from North American mountain sheep mitochondrial DNA. *Journal of Evolutionary Biology*, *19*(2), 419–430. doi: https://doi.org/10.1111/j.1420-9101.2005.01027.x

Lopes, F., Oliveira, L. R., Kessler, A., Crespo, E., Majluf, P., Sepúlveda, M., ... Bonatto, S. L. (2020). Gene-tree species-tree discordance in the eared seals is best explained by incomplete lineage sorting following explosive radiation in the southern hemisphere. *BioRxiv*. doi: https://doi.org/https://doi.org/10.1101/2020.08.11.246108

Lv, F. H., Peng, W. F., Yang, J., Zhao, Y. X., Li, W. R., Liu, M. J., ... Li, M. H. (2015). Mitogenomic meta-analysis identifies two phases of migration in the history of Eastern Eurasian sheep. *Molecular Biology and Evolution*, *32*(10), 2515–2533. doi: https://doi.org/10.1093/molbev/msv139

Martin, S. H., Most, M., Palmer, W. J., Salazar, C., McMillan, W. O., Jiggins, F. M., Jiggins, C. D. (2016). Natural Selection and Genetic Diversity in the Butterfly Heliconius melpomene. Genetics, 203(1), 525–541. doi: https://doi.org/10.1534/genetics.115.183285

McKay, B. S. (2018). Pigmentation and vision: Is GPR143 in control? *Journal of Neuroscience Research*, *97*(1), 77–87. doi: https://doi.org/10.1002/jnr.24246

Meadows, J. R. S., Hanotte, O., Drögemüller, C., Calvo, J., Godfrey, R., Coltman, D., ... Kijas, J. W. (2006). Globally dispersed Y chromosomal haplotypes in wild and domestic sheep. *Animal Genetics*, *37*(5), 444–453. doi: https://doi.org/10.1111/j.1365-2052.2006.01496.x

Mi, H., Dong, Q., Muruganujan, A., Gaudet, P., Lewis, S., & Thomas, P. D. (2010). PANTHER version 7: Improved phylogenetic trees, orthologs and collaboration with the Gene Ontology Consortium. *Nucleic Acids Research*, *38*(SUPPL.1), 204–210. doi: https://doi.org/10.1093/nar/gkp1019

Mi, H., Muruganujan, A., Ebert, D., Huang, X., & Thomas, P. D. (2019). PANTHER version 14: More genomes, a new PANTHER GO-slim and improvements in enrichment analysis tools. *Nucleic Acids Research*, *47*(D1), D419–D426. doi: https://doi.org/10.1093/nar/gky1038

Mi, H., Muruganujan, A., Huang, X., Ebert, D., Mills, C., Guo, X., & Thomas, P. D. (2019). Protocol Update for large-scale genome and gene function analysis with the PANTHER classification system (v.14.0). *Nature Protocols*, *14*(3), 703–721. doi: https://doi.org/10.1038/s41596-019-0128-8

Miller, J. M., Malenfant, R. M., David, P., Davis, C. S., Poissant, J., Hogg, J. T., ... & Coltman, D. W. (2014). Estimating genome-wide heterozygosity: Effects of demographic history and marker type. *Heredity*, *112*(3), 240–247. doi: https://doi.org/10.1038/hdy.2013.99

Miller, J. M., Poissant, J., Hogg, J. T., & Coltman, D. W. (2012). Genomic consequences of genetic rescue in an insular population of bighorn sheep (Ovis canadensis). *Molecular Ecology*, *21*(7), 1583–1596. doi: https://doi.org/10.1111/j.1365-294X.2011.05427.x

Ohbayashi, N., & Fukuda, M. (2020). Recent advances in understanding the molecular basis of melanogenesis in melanocytes. *F1000Research*, *9*, 1–10. doi: https://doi.org/10.12688/f1000research.24625.1

Palkopoulou, E., Lipson, M., Mallick, S., Nielsen, S., Rohland, N., Baleka, S., ... Reich, D. (2018). A comprehensive genomic history of extinct and living elephants. *Proceedings of the National Academy of Sciences of the United States of America*, *115*(11), E2566–E2574. doi: https://doi.org/10.1073/pnas.1720554115

Paradis, E., & Schliep, K. (2019). Ape 5.0: An environment for modern phylogenetics and evolutionary analyses in R. *Bioinformatics*, *35*(3), 526–528. doi: https://doi.org/10.1093/bioinformatics/bty633

Payseur, B. A., & Rieseberg, L. H. (2016). A genomic perspective on hybridization and speciation. *Molecular Ecology*, *25*(11), 2337–2360. doi: https://doi.org/10.1111/mec.13557

Pease, J. B., & Hahn, M. W. (2015). Detection and polarization of introgression in a five-taxon phylogeny. *Systematic Biology*, *64*(4), 651–662. doi: https://doi.org/10.1093/sysbio/syv023

Pertea, G., & Pertea, M. (2020). GFF Utilities: GffRead and GffCompare. *F1000Research*, *9*, 1–20. doi: https://doi.org/10.12688/f1000research.23297.2

Poelstra, J. W., Vijay, N., Bossu, C. M., Lantz, H., Ryll, B., Müller, I., ... Wolf, J. B. W. (2014). The genomic landscape underlying phenotypic integrity in the face of gene flow in crows. *Science*, *344*(6190), 1410–1414. doi: https://doi.org/10.1126/science.1253226

Purcell, S., Chang, C. (2019, December). *PLINK 2.0* [Software]. Retrieved from www.cog-genomics.org/plink/2.0/

Quinlan, A. R., & Hall, I. M. (2010). BEDTools: A flexible suite of utilities for comparing genomic features. *Bioinformatics*, *26*(6), 841–842. doi: https://doi.org/10.1093/bioinformatics/btq033

Rambaut, A., Drummond, A. J., Xie, D., Baele, G., & Suchard, M. A. (2018). Posterior summarization in Bayesian phylogenetics using Tracer 1.7. *Systematic Biology*, *67*(5), 901–904. doi: https://doi.org/10.1093/sysbio/syy032

Ramos-Lopez, O., Riezu-Boj, J. I., Milagro, F. I., Zulet, M. A., Santos, J. L., & Martinez, J. A. (2019). Associations between olfactory pathway gene methylation marks, obesity features and dietary intakes. *Genes & Nutrition*, *14*(1), 11. doi: https://doi.org/10.1186/s12263-019-0635-9

R Core Team. (2020). *R: A language and environment for statistical computing* [Software]. Vienna, AT: R Foundation for Statistical Computing. Retrieved from https://www.R-project.org/

Rezaei, H. R., Naderi, S., Chintauan-Marquier, I. C., Taberlet, P., Virk, A. T., Naghash, H. R., ... Pompanon, F. (2010). Evolution and taxonomy of the wild species of the genus Ovis (Mammalia, Artiodactyla, Bovidae). *Molecular Phylogenetics and Evolution*, *54*(2), 315–326. doi: https://doi.org/10.1016/j.ympev.2009.10.037

Rimmer, A., Phan, H., Mathieson, I., Iqbal, Z., Twigg, S. R. F., Wilkie, A. O. M., ... Lunter, G. (2014). Integrating mapping-, assembly- and haplotype-based approaches for calling variants in clinical sequencing applications. *Nature Genetics*, *46*(8), 912–918. doi: https://doi.org/10.1038/ng.3036

Rochus, C. M., Tortereau, F., Plisson-Petit, F., Restoux, G., Moreno-Romieux, C., Tosser-Klopp, G., & Servin, B. (2018). Revealing the selection history of adaptive loci using genome-wide scans for selection: An example from domestic sheep. *BMC Genomics*, *19*(1), 1–17. doi: https://doi.org/10.1186/s12864-018-4447-x

Rochus, C. M., Westberg Sunesson, K., Jonas, E., Mikko, S., & Johansson, A. M. (2019). Mutations in *ASIP* and *MC1R*: dominant black and recessive black alleles segregate in native Swedish sheep populations. *Animal Genetics*, *50*(6), 712–717. doi: https://doi.org/10.1111/age.12837

RStudio Team. (2020). *RStudio: Integrated development environment for R* [Software]. Boston, MA: RStudio, PBC. Retrieved from http://www.rstudio.com/

Serre, C., Busuttil, V., & Botto, J. M. (2018). Intrinsic and extrinsic regulation of human skin melanogenesis and pigmentation. *International Journal of Cosmetic Science*, *40*(4), 328–347. doi: https://doi.org/10.1111/ics.12466

Shannon, P., Markiel, A., Ozier, O., Baliga, N. S., Wang, J. T., Ramage, D., ... Ideker, T. (2003) Cytoscape: A software environment for integrated models of biomolecular interaction networks. *Genome Research*, *13*(11), 2498–2504. doi: https://doi.org/10.1101/gr.1239303

Shurtliff, Q. R. (2013). Mammalian hybrid zones: A review. *Mammal Review*, *43*(1), 1–21. doi: https://doi.org/10.1111/j.1365-2907.2011.00205.x

Sim, Z., Hall, J. C., Jex, B., Hegel, T. M., Coltman, D. W. (2016) Genome-wide set of SNPs reveals evidence for two glacial refugia and admixture from postglacial recolonization in an alpine ungulate. *Molecular Ecology*, *25*(15), 3696-3705. doi: https://doi.org/10.1111/mec.13701

Sitaram, A., & Marks, M. S. (2012). Mechanisms of protein delivery to melanosomes in pigment cells. *Physiology*, *27*(2), 85–99. doi: https://doi.org/10.1152/physiol.00043.2011

Solís-Lemus, C., Yang, M., & Ané, C. (2016). Inconsistency of species tree methods under gene flow. *Systematic Biology*, *65*(5), 843–851. doi: https://doi.org/10.1093/sysbio/syw030

Soltis P. S., Soltis D. E. (2003). Applying the bootstrap in phylogeny reconstruction. *Statistical Science*. 18(2), 256–267. doi: https://doi.org/10.1214/ss/1063994980.

Somenzi, E., Ajmone-Marsan, P., & Barbato, M. (2020). Identification of ancestry informative marker (AIM) panels to assess hybridisation between feral and domestic sheep. *Animals*, *10*(4). doi: https://doi.org/10.3390/ani10040582

Stamatakis, A. (2014). RAxML version 8: A tool for phylogenetic analysis and post-analysis of large phylogenies. *Bioinformatics*, *30*(9), 1312–1313. doi: https://doi.org/10.1093/bioinformatics/btu033

Storey, J. D., Bass, A. J., Dabney, A., Robinson, D. (2020). *qvalue: Q-value estimation for false discovery rate control* [R package version 2.22.0]. Retrieved from http://github.com/jdstorey/qvalue

Sturm, R. A., & Duffy, D. L. (2012). Human pigmentation genes under environmental selection. *Genome Biology*, *13*(9). doi: https://doi.org/10.1186/gb-2012-13-9-248

Szklarczyk, D., Franceschini, A., Wyder, S., Forslund, K., Heller, D., Huerta-Cepas, J., ... Von Mering, C. (2015). STRING v10: Protein-protein interaction networks, integrated over the tree of life. *Nucleic Acids Research*, *43*(D1), D447–D452. doi: https://doi.org/10.1093/nar/gku1003

Talla, V., Soler, L., Kawakami, T., Dinca V., Vila, R., Friberg, M., Wiklund, C., ... Gonzalez, J. (2019). Dissecting the Effects of Selection and Mutation on Genetic Diversity in Three Wood White (Leptidea) Butterfly Species. *Genome Biology and Evolution*, *11*(10), 2875–2886. doi: https://doi.org/10.1093/gbe/evz212

Than, C., Ruths, D., & Nakhleh, L. (2008). PhyloNet: A software package for analyzing and reconstructing reticulate evolutionary relationships. *BMC Bioinformatics*, *9*, 1–16. doi: https://doi.org/10.1186/1471-2105-9-322

Thomas, P. D., Campbell, M. J., Kejariwal, A., Mi, H., Karlak, B., Daverman, R., ... Narechania, A. (2003). PANTHER: A library of protein families and subfamilies indexed by function. *Genome Research*, *13*(9), 2129–2141. doi: https://doi.org/10.1101/gr.772403

Upadhyay, M., Hauser, A., Kunz, E., Krebs, S., Blum, H., Dotsev, A., ... Medugorac, I. (2020). The First Draft Genome Assembly of Snow Sheep (Ovis nivicola). *Genome Biology and Evolution*, *12*(8), 1330–1336. doi: https://doi.org/10.1093/gbe/evaa124

Vianna, J. A., Fernandes, F. A. N., Frugone, M. J., Figueiró, H. V., Pertierra, L. R., Noll, D., ... Bowie, R. C. K. (2020). Genome-wide analyses reveal drivers of penguin diversification. *Proceedings of the National Academy of Sciences of the United States of America*, *117*(36), 22303–22310. doi: https://doi.org/10.1073/pnas.2006659117

Wasmeier, C., Romao, M., Plowright, L., Bennett, D. C., Raposo, G., & Seabra, M. C. (2006). Rab38 and Rab32 control post-Golgi trafficking of melanogenic enzymes. *Journal of Cell Biology*, *175*(2), 271–281. doi: https://doi.org/10.1083/jcb.200606050

Wen, D., Yu, Y., Zhu, J., & Nakhleh, L. (2018). Inferring phylogenetic networks using PhyloNet. *Systematic Biology*, *67*(4), 735–740. doi: https://doi.org/10.1093/sysbio/syy015

Wickham, H. (2016). *ggplot2: Elegant graphics for data analysis*. Springer-Verlag New York. Retrieved from https://ggplot2.tidyverse.org

Won, H., Lee, H. R., Gee, H. Y., Mah, W., Kim, J. I., Lee, J., ... Kim, E. (2012). Autistic-like social behaviour in Shank2-mutant mice improved by restoring NMDA receptor function. *Nature*, *486*(7402), 261–265. doi: https://doi.org/10.1038/nature11208

Worley, K., Strobeck, C., Arthur, S., Carey, J., Schwantje, H., Veitch, A., & Coltman, D. W. (2004). Population genetic structure of North American thinhorn sheep (Ovis dalli). *Molecular Ecology*, *13*(9), 2545–2556. doi: https://doi.org/10.1111/j.1365-294X.2004.02248.x

Wu, C. C., Klaesson, A., Buskas, J., Ranefall, P., Mirzazadeh, R., Söderberg, O., & Wolf, J. B. W. (2019). In situ quantification of individual mRNA transcripts in melanocytes discloses gene regulation of relevance to speciation. *Journal of Experimental Biology*, *222*(5). doi: https://doi.org/10.1242/jeb.194431

Xin, L., Yang, J., Shen, M., Xie, X-L., Liu, G-J., Xu, Y-X., ... Li, M-H. (2020). Whole-genome resequencing of wild and domestic sheep identifies genes associated with morphological and agronomic traits. *Nature communications*, *11*(2815). doi: https://doi.org/10.1038/s41467-020-16485-1

Xu, Z., Chen, L., Jiang, M., Wang, Q., Zhang, C., & Xiang, L. F. (2018). CCN1/Cyr61 Stimulates Melanogenesis through Integrin α6β1, p38 MAPK, and ERK1/2 Signaling Pathways in Human Epidermal Melanocytes. *Journal of Investigative Dermatology*, *138*(8), 1825–1833. doi: https://doi.org/10.1016/j.jid.2018.02.029

Yang, Z. (2007). PAML 4: Phylogenetic analysis by maximum likelihood. *Molecular Biology and Evolution*, *24*(8), 1586–1591. doi: https://doi.org/10.1093/molbev/msm088

Yang, Z., dos Reis, M. (2010). Statistical properties of the branch-site test of positive selection. *Molecular Biology and Evolution*, *28*(3), 1217–1228. doi: https://doi.org/10.1093/molbev/msq303

Young, A. D., Gillung, J. P. (2019). Phylogenomics - principles, opportunities and pitfalls of big-data phylogenetics. *Systematic Entomology*, 45, 225–247. doi: https://doi.org/10.1111/syen.12406

Zhang, C., Rabiee, M., Sayyari, E., & Mirarab, S. (2018). ASTRAL-III: Polynomial time species tree reconstruction from partially resolved gene trees. *BMC Bioinformatics*, *19*(Suppl 6), 15–30. doi: https://doi.org/10.1186/s12859-018-2129-y

Data Accessibility

All whole-genome short-read sequences of the six bighorn and four thinhorn sheep individuals were obtained in collaboration with professor Menghua Li's research group (Chen, Xu, & Li, unpublished). Sequence submission to a public domain (NCBI) will happen after the publication

of the work Chen, Xu, & Li. The domestic sheep assembly (NCBI accession no. GCA_002742125.1), as well as snow sheep (NCBI accession no. ERX4127321; Upadhyay et al., 2020) and goat (NCBI accession no. SRX1918187; SRX1890394) short-read sequences were obtained from NCBI.

Author Contributions

- Conceptualization: SHDS, DWC
- Data curation: SHDS, MHL, FL, XL, AD, RMP, JMM
- Formal analysis and investigation: SHDS RMP, JMM
- Writing - original draft preparation: SHDS
- Writing - review and editing: AD, DWC, FL, JMM, MHL, RMP, and XL
- Funding acquisition: DWC, MHL
- Resources: DWC, MHL

Tables and Figures

Table 1. Datasets and respective subsets used in each analysis.

Dataset	Subset	GF size	GF step size	Thinhorn	Bighorn	Snow	Domestic sheep	Goat	Number of individuals	Analyses
1	1.1	10-kb	None†		B1-6				6	a
1	1.2	10-kb	None†	D1, S1-3					4	a
2	2.1	1-Mb	6-kb	D1, S1-3	B1-6	SN	DS		12	b, c
2	2.2	1-Mb	100-kb	D1, S1-3	B1-6	SN	DS		12	b, c
2	2.3	1-Mb	200-kb	D1, S1-3	B1-6	SN	DS		12	b, c
3	3.1	100-kb	6-kb	D1, S1-3	B1-6	SN	DS		12	b, c

3	3.2	100-kb	100-kb	D1, S1-3	B1-6	SN	DS		12	b, c
3	3.3	100-kb	200-kb	D1, S1-3	B1-6	SN	DS		12	b, c
4	4.1	10-kb	6-kb	D1, S1-3	B1-6	SN	DS		12	b, c
4	4.2	10-kb	100-kb	D1, S1-3	B1-6	SN	DS		12	b, c
4	4.3	10-kb	200-kb	D1, S1-3	B1-6	SN	DS		12	b, c
5	5.1	10-kb	6-kb	D1, S1	B4, B6	SN	DS		6	b, c
5	5.2	10-kb	100-kb	D1, S1	B4, B6	SN	DS		6	b, c, d
5	5.3	10-kb	200-kb	D1, S1	B4, B6	SN	DS		6	b, c, d
6	6.1	10-kb	6-kb	D1, S1	B4, B6	SN	DS	GO	7	b, c
6	6.2	10-kb	100-kb	D1, S1	B4, B6	SN	DS	GO	7	b, c
6	6.3	10-kb	200-kb	D1, S1	B4, B6	SN	DS	GO	7	b, c
7	7.1	10-kb	6-kb	D1, S1	B6	SN	DS		5	b, c
7	7.2	10-kb	100-kb	D1, S1	B6	SN	DS		5	b, c,
7	7.3	10-kb	200-kb	D1, S1	B6	SN	DS		5	b, c, e
8	8.1-8.15	100-kb	None†	S1, S2	B1-6		DS		5	f
9	9.1-9.15	100-kb	None†	S1, S3	B1-6		DS		5	f
10	10.1-10.15	100-kb	None†	S2, S3	B1-6		DS		5	f
11	11.1-11.15	100-kb	None†	D1, S1	B1-6		DS		5	f
12	12.1-12.15	100-kb	None†	D1, S2	B1-6		DS		5	f
13	13.1-13.15	100-kb	None†	D1, S3	B1-6		DS		5	f
14	14.1-14.6	100-kb	None†	D1, S1	B1-6		DS		4	g
15	15.1-15.6	100-kb	None†	D1, S2	B1-6		DS		4	g
16	16.1-16.6	100-kb	None†	D1, S3	B1-6		DS		4	g

†Non-overlapping windows with no step size.
D1: Dall; S(1-3): Stone; B(1-6): bighorn; DS: domestic sheep; GO: goat.
a: nucleotide diversity; b: phylogenomic analyses; c: consensus species tree estimate; d: divergence time and absolute divergence; e: reticulate evolution analyses; f: 5-taxon introgression analyses; g: 4-taxon introgression analyses.

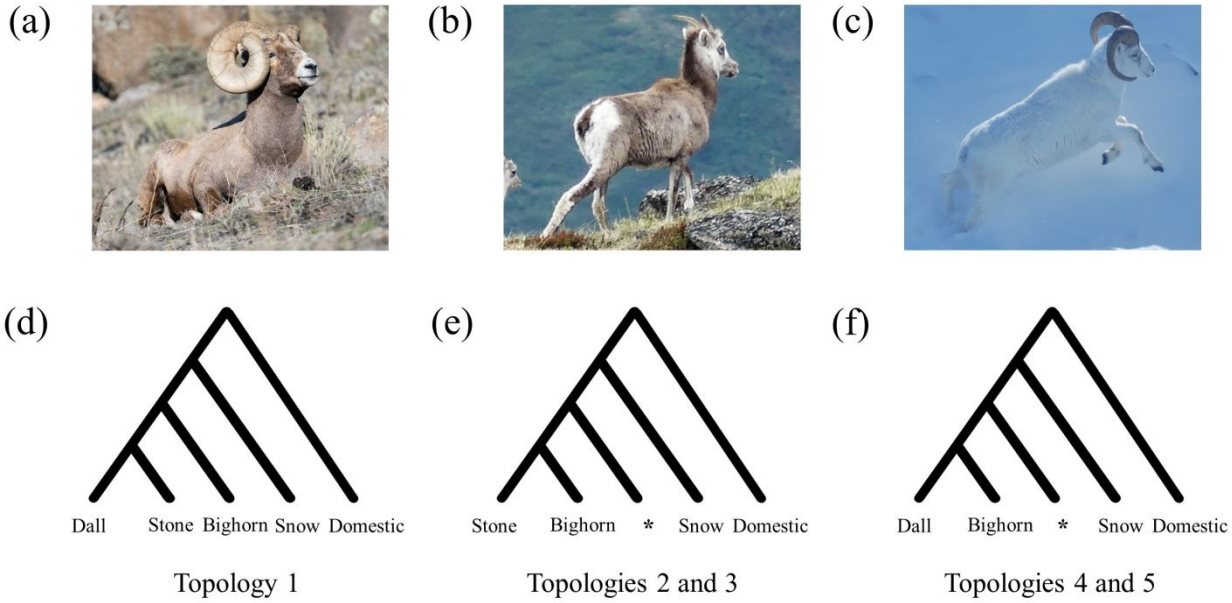

Figure 1. Evolutionary relationships among Pachyceriforms. The coat color patterns of (a) bighorn (public domain), (b) Stone (Photo credit: Krystal Kriss), and (c) Dall (Photo credit: Bill Jex) sheep might be related to their speciation mode (d-f). The different topologies place either Dall and Stone (d: topology 1), Stone and bighorn (e: topologies 2-3) or Dall and bighorn (f: topologies 4-5) as sister clades. * represents any other possible combination of bighorn or thinhorn individuals, considering snow and domestic sheep as outgroups to the focal species.

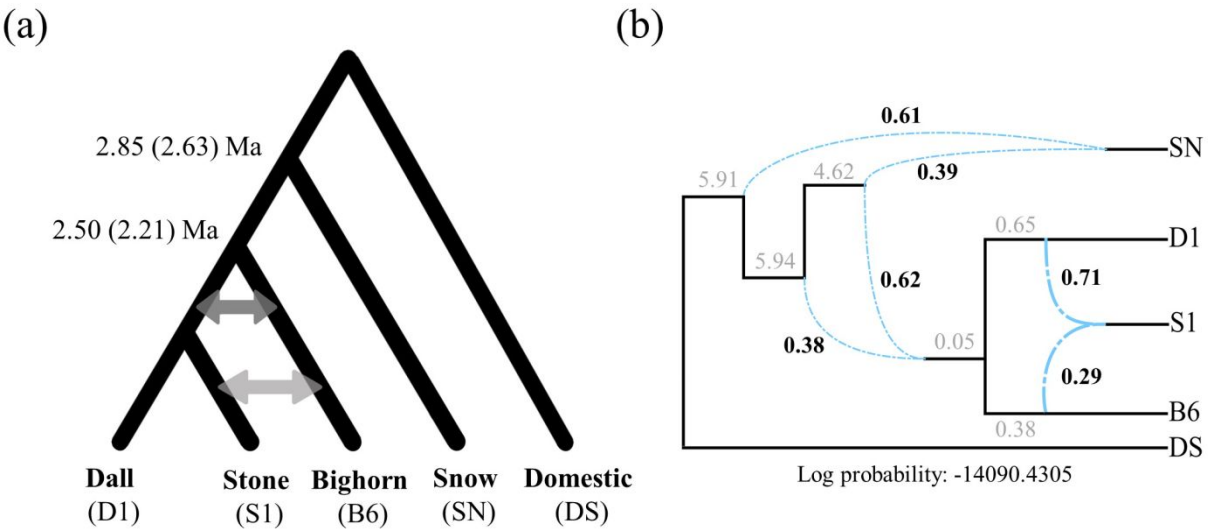

Figure 2. Speciation reconstruction of Pachyceriforms. (a) Species tree showing the divergence times estimated for GFs with 100 and 200-kb step size, respectively. Arrows indicate potential ancient hybridization between the thinhorn lineage and bighorn, as well as Stone and bighorn. (b) Best network reconstructed from a maximum-likelihood approach in PhyloNet. Gray values are branch-lengths in coalescent units. Blue lines represent reticulation edges with bold values showing their inheritance probabilities. The log probability is shown below the network (see Table S9 for the information criterion test).

(a)

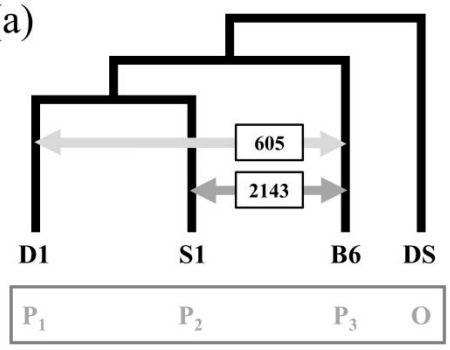

(b)

Gene name	Introgression pattern	Function	Reference
AP1S1	D1 ↔ B6	Protein deliver to melanosome	Serre et al., 2018
CCN1	D1 ↔ B6	Activation of melanogenesis	Xu et al., 2018
CTNS	D1 ↔ B6	Control of skin and hair pigmentation	Chiaverini et al., 2012
GPR143	D1 ↔ B6	Melanosome biogenesis and structure	Filippo, Manga, & Schiedel, 2017
MC5R	D1 ↔ B6	Pigment-dispersing activities	Kobayashi et al., 2012
TCF7L2	D1 ↔ B6	Melanogenesis pathway	Kanehisa, 2019; Kanehisa et al., 2019, 2020
ADCY5	S1 ↔ B6	Melanogenesis pathway	Kanehisa, 2019; Kanehisa et al., 2019, 2020
ADCY7	S1 ↔ B6	Melanogenesis pathway	Kanehisa, 2019; Kanehisa et al., 2019, 2020
ADCY8	S1 ↔ B6	Melanogenesis pathway	Kanehisa, 2019; Kanehisa et al., 2019, 2020
CALML4	S1 ↔ B6	Melanogenesis pathway	Kanehisa, 2019; Kanehisa et al., 2019, 2020
CALML6	S1 ↔ B6	Melanogenesis pathway	Kanehisa, 2019; Kanehisa et al., 2019, 2020
CAMK2D	S1 ↔ B6	Melanogenesis pathway	Kanehisa, 2019; Kanehisa et al., 2019, 2020
CTNNB1	S1 ↔ B6	Melanogenesis pathway	Kanehisa, 2019; Kanehisa et al., 2019, 2020
DTNBP1	S1 ↔ B6	Membrane trafficking in melanosome biogenesis	Sitaram & Marks, 2012
FZD3	S1 ↔ B6	Melanogenesis pathway	Kanehisa, 2019; Kanehisa et al., 2019, 2020
FZD9	S1 ↔ B6	Melanogenesis pathway	Kanehisa, 2019; Kanehisa et al., 2019, 2020
HPS4	S1 ↔ B6	Melanosome biogenesis	Ohbayashi & Fukuda, 2020
MAP2K2	S1 ↔ B6	Melanogenesis pathway	Kanehisa, 2019; Kanehisa et al., 2019, 2020
MREG	S1 ↔ B6	Melanosome transport	Ohbayashi & Fukuda, 2020
PLCB3	S1 ↔ B6	Melanogenesis pathway	Kanehisa, 2019; Kanehisa et al., 2019, 2020
PLCB4	S1 ↔ B6	Melanogenesis pathway	Kanehisa, 2019; Kanehisa et al., 2019, 2020
POMC	S1 ↔ B6	Melanogenesis pathway	Kanehisa, 2019; Kanehisa et al., 2019, 2020
PRKCA	S1 ↔ B6	Melanogenesis pathway	Kanehisa, 2019; Kanehisa et al., 2019, 2020
PRKCE	S1 ↔ B6	Regulation of melanogenesis by the protein kinase-dependent pathway	D'Mello, et al., 2016; Gordon & Gilchrest, 1999
PRKCG	S1 ↔ B6	Melanogenesis pathway	Kanehisa, 2019; Kanehisa et al., 2019, 2020
RAB32	S1 ↔ B6	Melanosome biogenesis	Ohbayashi & Fukuda, 2020
SOX10	S1 ↔ B6	Melanocyte development	Harris et al., 2010
TYR	S1 ↔ B6	Pigment regulation	Koseniuk et al., 2018

(c)

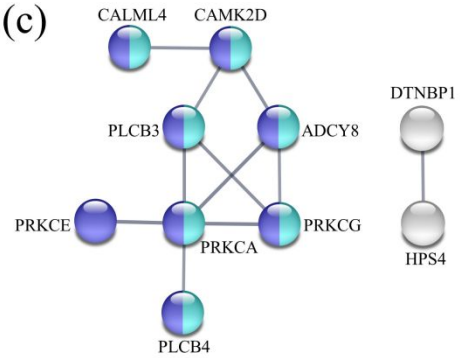

Figure 3. Introgression analysis and its relation to potential adaptive genes. (a) 4-taxon D-statistics analysis of subset 14.6, where the number of windows represents the introgression signal between Dall (D1↔B6) or Stone (S1↔B6) and bighorn. (b) Coat color genes within the D-statistics GFs and their respective function(s). These genes are listed by their introgression signal observed (i.e., D1↔B6), and highlighted genes in grey are also present within the 4-taxon combined dataset. (c) Protein-protein interaction network of genes present within GFs with introgression signal between S1 and B6. Light blue genes are directly part of the melanogenesis pathway, as well as three other pathways (see Table S13). Dark blue genes are involved in the aldosterone synthesis and secretion, and inflammatory mediator regulation of TRP channel. Gray genes are a local network cluster associated with the biogenesis of lysosomal organelle complex. Disconnected genes are not shown (see Table S13 for the full gene list per pathway observed).

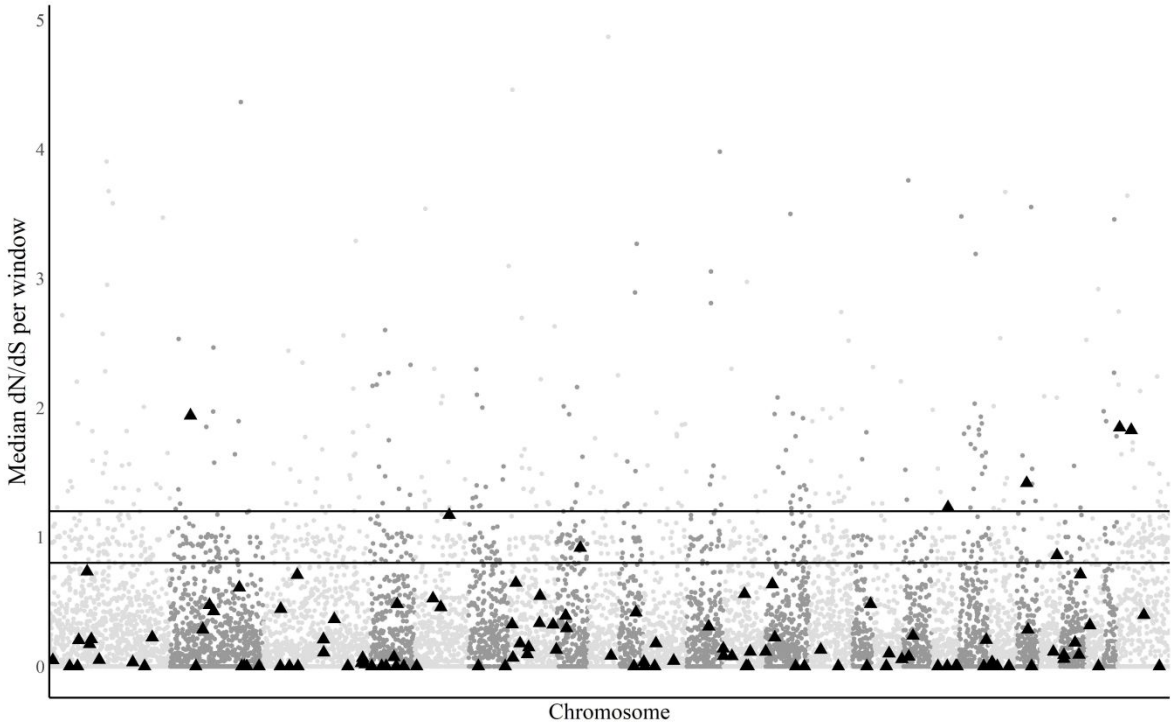

Figure 4. Plot of median ω values per 100-kb window. Chromosomes are ordered from 1 to 26 followed by X at the far right and alternate grayscale colors. Windows that contain a coat color gene are highlighted as black triangles. The cutoff lines, from bottom to top, separate purifying, neutral, and positive selection.